A New Research Proposal submitted to JLab PAC30

Nucleon Resonance Studies with CLAS12 in the Transition from Soft to Partonic Physics

T. S. H. Lee
Argonne National Lab,USA

H. Avakian, V.D. Burkert[*], *L. Elouadrhiri, V.I. Mokeev*[*,†], *S. Stepanyan*
Jefferson Lab, Newport News, VA 23606, USA

V.V. Chesnokov, G.V. Fedotov, B.S. Ishkhanov, E.L. Isupov, N.V.Shvedunov
Skobeltsyn Nuclear Physics Institute, Moscow State University, 11989 Moscow, Russia

W. Roberts
Physics Department, Florida State University, Tallahassee, Florida 32306, USA

V. Kubarovsky, P. Stoler[*]
Department of Physics, Rensselaer Polytechnic Institute, Troy, NY 12181, USA

K. Joo[*], *N. Markov, T. Mineeva, M. Ungaro*
University of Connecticut, Storrs, Connecticut 06269, USA

C. Djalali, R.W. Gothe[*,†], *J. Langheinrich, K. Park, S. Strauch, D. Tedeschi*
Department of Physics and Astronomy, University of South Carolina, Columbia, SC 29208, USA

I. Aznauryan
Yerevan Physics Institute, 375036 Yerevan, Armenia

A. Biselli
Physics Department, Fairfield University, Fairfield, CT 06824, USA

W.J. Briscoe, I. Strakovsky
Center for Nuclear Studies, Department of Physics, The George Washington University, Washington, D.C. 20052, USA

and the CLAS collaboration

[*] *Spokesperson*
[†] *Contact person*

Abstract

We plan to measure exclusive single-pion and double-pion electro-production off a proton target to study the nucleon resonances with the CLAS12 detector and the energy upgraded CEBAF beam. Exclusive final states will be measured including the identification of π^0 and η mesons by measuring the two decay photons as well as of charged pions. In the proposed measurements, we expect to obtain electromagnetic transition form factors for well established excited nucleon states in the unexplored domain of Q^2, from 4 to 14 GeV^2. The aim of the measurements is to explore the transition from the hadronic to the partonic regime. In parallel, a major coupled-channel approach is under development to extract the resonance electro-couplings from the expected extensive data. This experiment is part of the comprehensive program of measurements of exclusive electro-production with CLAS12, in which various channels such as deeply virtual Compton scattering and deeply virtual exclusive meson production, will be measured as well. By providing a high statistics and high quality of analysis of the proposed measurements, significant new information on the mechanisms of QCD confinement in hadrons with three valence quark will be obtained.

Contents

1 Technical Participation of Research Groups

1.1 University of South Carolina

The University of South Carolina group is actively involved in this proposal using CLAS12 base equipment. Ralf Gothe is a member of the CLAS12 Steering Committee. Among the CLAS12 baseline equipment, our group has taken responsibility for the design, prototyping, construction and testing of the forward Time-of-Flight detector ToF12. Ralf Gothe is currently heading Time-of-Flight technical working group. Three USC faculty members (R. Gothe, S. Strauch, and D. Tedeschi), one post-doc (K. Park), three graduate (L. Graham, H. Lu, and Z.Zhao) and two undergraduate students (E. Phelps and D. Gothe) are already working on this project. The USC nuclear physics group is committed to carry out this project and will continue to be fully involved as needed. The group is currently funded by NSF. The University of South Carolina is providing a detector assembly hall for the duration of the project and has funded $ 60,000 for the initial infrastructural needs. Additional sources of funding will be sought as appropriate.

Beyond the baseline equipment, the group is also deeply involved in software planning and development for CLAS12. Joern Langheinrich is currently leading the efforts to develop a Monte-Carlo simulation for the CLAS12 detector.

1.2 Moscow State University

The Moscow State University Group (MSU) is actively involved in development of CLAS12 base equipment needed for proposed experiments.

In particular, the MSU group will participate in development of the simulation (GEANT4) and reconstruction software and trigger and data acquisition. The MSU group takes responsibility for the maintenance and development of the special Data Base needed for N* studies in coupled channel analysis. This Project will be developed jointly with Hall B and EBAC. MSU personnel will also participate in the development of the pre-shower calorimeter, the HTTC and drift chambers under supervision of Hall B staff. At least 4 staff scientist and 5 PhD and/or graduate students will be involved in base equipment development.

1.3 Rensselaer Polytechnic Institute

The RPI group is actively involved in this proposal using CLAS12 base equipment. Paul Stoler is a member of the CLAS12 Steering Committee. Among the CLAS12 baseline equipment, our group has involved in the design, prototyping, construction and testing of the high threshold and modification of the low threshold Cerenkov detector. Currently, Paul Stoler is serving as a coordinator for the collaboration of groups involved in the effort. Valery Kubarovsky is designing and building the apparatus for testing the prototype components. Two undergraduates Jason Sanchez and Stephanie Tomasulo, are spending the summer at JLab working respectively on prototype mirror fabrication and computer aided optics design

and simulation. The group will continue to be fully involved as needed. The group is currently funded by NSF and RPI. Additional sources of funding will be sought as appropriate.

1.4 University of Connecticut

The University of Connecticut (UConn) group is actively involved in this proposal using CLAS12 baseline equipment.

Among the CLAS 12 baseline equipment, our group has taken responsibility for the design, prototyping, construction and testing of the high threshold Cerenkov counter (HTCC). One faculty member, one post-doc, four graduate students are already or will be working at least part time on this project in the next few years. The University of Connecticut Research Foundation (UCRF) already funded $32,000 for the equipment purchase for the HTCC prototyping project. The University is also providing funding for a half postdoctoral support and a half graduate student support for the next two years for the our group's JLab research activities. The group is currently funded by the U.S Department of Energy (DOE). Additional sources of funding will be sought as appropriate.

Beyond the baseline equipment, the group is also deeply involved in software planning and development for CLAS12. The group was recently awarded a DOE SBIR/STTR Phase I grant with a software company, CyberConnect EZ to develop a software framework to archive a large scale nuclear physics experiment data base

2 Introduction

Nucleons, and baryons in general, have played an important role in the development of the quark model and of QCD. The concept of quarks was first made manifest through the study of baryon spectroscopy. For many years the properties of the ground state and the excited states of baryons had been treated in terms of isobars or constituent quarks. However, currently we are at the threshold of a new era in describing these states in terms of QCD degrees of freedom. Recent QCD calculations on the lattice[6] show evidence for the "Y-shape" color flux indicating a genuine 3-body force for baryons with stationary quarks as shown in Fig. 1. A dominant 2-body force would generate Δ-shape color flux. This 3-body force is a unique feature of a 3-quark baryon system in QCD. Lattice simulations[7] also relate the fundamental QCD Lagrangian to quark confinement potentials. So far ground and first excited flux tube potentials are available. These potentials are responsible for the formation of the ground state and a variety of excited nucleon states, and determine the behavior of N^* electromagnetic transition form factors as a function of the distance scale. In turn, the resonance transition form factors carry information that is sensitive to the underlying potential. In the proposed measurements we expect to obtain electromagnetic transition form factors for the well established excited nucleon states with significant electromagnetic couplings in a wide range of photon virtualities, Q^2.

Studying the nucleon ground state in elastic electron scattering allows us to determine the charge and magnetic moment distribution in the nucleon. By exciting the nucleon into resonant states through the transfer of energy and angular momentum and studying their excitation strength versus the distance scale we can expect to learn a great deal about the interquark potential, and how confinement works in hadrons with 3 valence quarks. At this

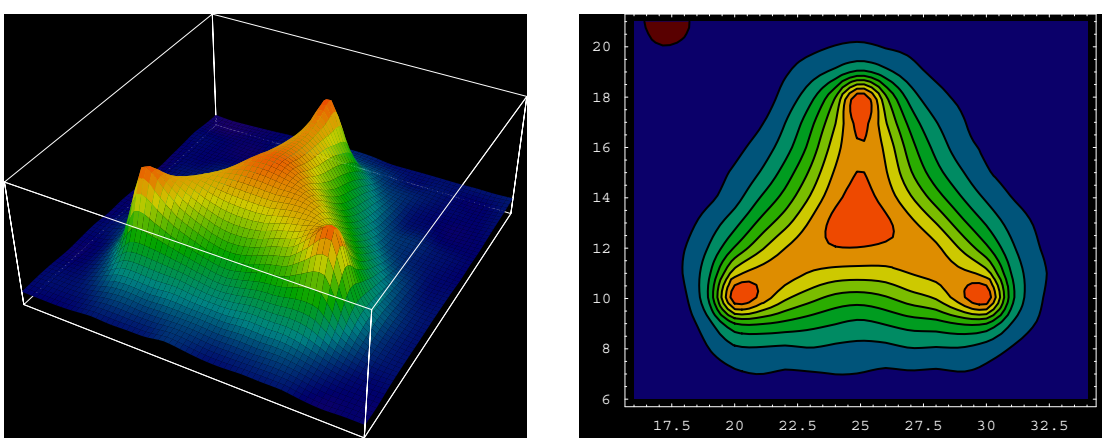

Figure 1: Lattice QCD calculation of the 3D color flux distribution for a baryon. The calculation was carried out to study the abelian color-flux distribution in a static 3-quark system. The "Y-shape" configuration is evident, indicating the presence of a genuine 3-body force. The graph shows high density at the quark locations and in the center. The Δ-shaped flux configuration, characteristic of 2-body forces would have a depletion in the center.

point lattice simulations may be directly tested against the wealth of phenomenological data on the internal N^* structure.

Nucleon resonances are clearly seen in inelastic inclusive structure functions off nucleons in the entire kinematic range covered by existing measurements. Moreover, the Q^2 evolution of the non-resonant parts in inclusive structure functions may be described reasonably well by QCD based approaches, while the evolution of the N^* excitation strength with Q^2 strongly depends on the quantum numbers of the excited state [11].

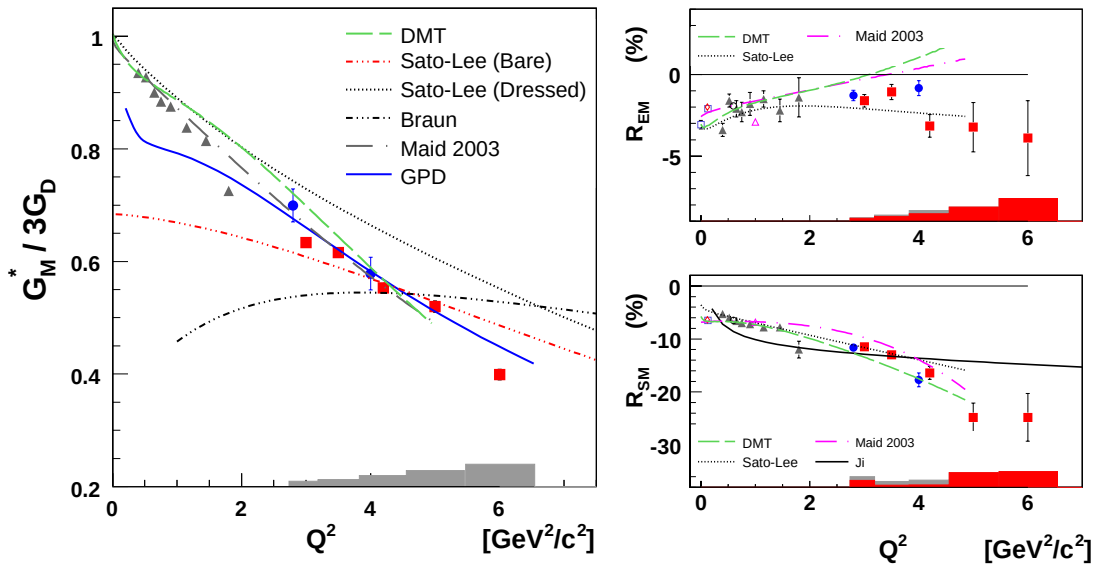

Figure 2: *Left panel*: The $N\Delta(1232)$ transition form factor $G_M^*/3G_D$ [110]. *Right panels*: The ratios R_{EM} (upper panel) and R_{SM} (lower panel) [110]. The data are from Jlab, Mami and Bates.

The CLAS12 detector, coupled with the unprecedented quality of the upgraded CEBAF beam, will be the only facility worldwide capable of accessing the N^* transition form factors in the unexplored domain of high Q^2, from 4 to 14 GeV^2.

In order to study nucleon excitations through the quark core we have to probe the nucleon at short enough distances where the quarks no longer appear "dressed" with $q\bar{q}$ pairs and act as effective degrees of freedom, or "constituent" quarks. In the language of dynamical models with hadronic degrees of freedom, the quark "dressing" is usually referred to as the nucleons "meson cloud". The effect of the meson cloud on the nucleon's response to electromagnetic probes makes the interpretation of N* excitations in terms of the quark substructure ambiguous or model-dependent at best. In the following section we will argue, based on recent dynamical model calculations as well as on Lattice QCD calculations, and backed up by empirical evidence, that currently available momentum transfers in electron scattering are insufficient to fully penetrate through the meson cloud to the nucleon's quark core, and that the energy and momentum transfer available with the 12 GeV upgrade are required to obtain the necessary resolving power.

2.1 Penetrating the meson cloud

The effort of the CLAS collaboration in studying nucleon resonance transitions at increasingly short distances has resulted in strong empirical evidence of large meson contributions to the resonance excitations at large and medium distances. This is particularly evident in the region of the $\gamma^* N\Delta$ transition where constituent quark models using point-like $\gamma^* - q$ couplings are unable to explain the considerably larger strength of the magnetic dipole transition from what is predicted from quark contributions alone. Also, the electric quadrupole transition moment usually expressed through the ratio $R_{EM} = E_{1+}/M_{1+}$ at the resonance pole, is much larger (typical accepted $R_{EM} \approx -2.5\% \pm 0.5\%$ [14]) compared to the predicted $R_{EM}^{CQM} < 0.5\%$. This is shown in Figure 2, where the magnetic transition form factor is displayed in the right panel. The effect of the meson cloud is estimated at 30% for $Q^2 = 0$, and at 15% for $Q^2 = 5\text{GeV}^2$. In terms of resonance strength the effect is 50% and 25%, respectively.

In the region of the Roper resonance $P_{11}(1440)$, the transverse transition amplitude $A_{1/2}(Q^2)$ shows a strong Q^2 dependence at small photon virtualities, even changing sign in the range $Q^2 = 0.5 - 1$ GeV^2. Moreover, the longitudinal transition amplitude $S_{1/2}$ is large at small Q^2, also indicating strong hadronic contributions to the resonance transition strength. This empirical information is best explained by large meson cloud effects. It is also supported by calculations within the chiral quark model [15] that discuss the role of these $q\bar{q}$ components in the wave function of the excited states, as well as of the nucleon. In these models, the Roper resonance has a large nucleon-meson component of 30% or more, with the remaining 70% induced by interactions with the quarks. In other models [28], the Roper resonance couples through vector mesons to the photon, generating a characteristic Q^2-dependence for the transition amplitudes.

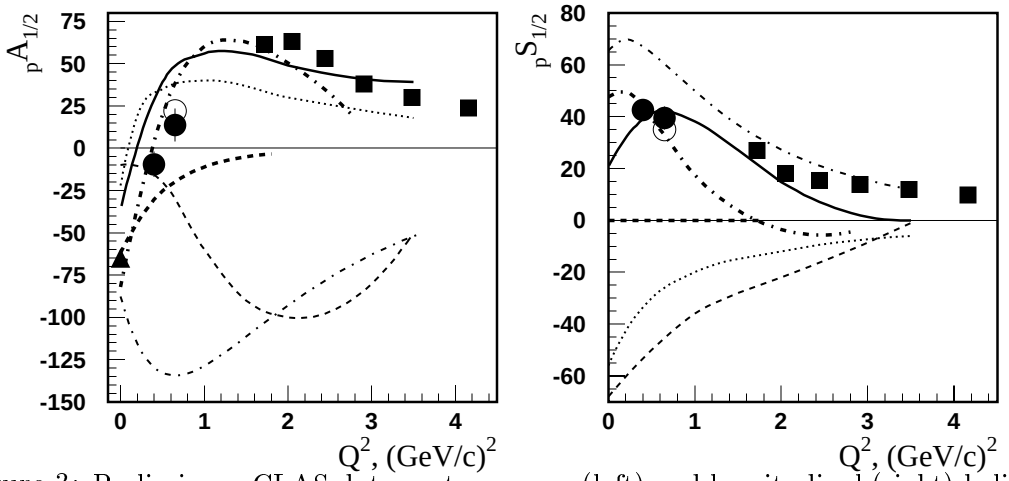

Figure 3: Preliminary CLAS data on transverse (left) and longitudinal (right) helicity amplitudes for the $P_{11}(1440)$. Model calculations are from [26–28, 71, 112]. The low Q^2 behavior and transition region is best described by the meson cloud model of [28], while the high Q^2 behavior is consistent with the light cone quark model [71].

The empirical evidence shows that the meson contributions are not only peripheral but extend to rather short distances although with decreasing strength. In the $\Delta(1232)$ region dynamical hadron models that take meson effects into account show that the meson cloud still plays an important though reduced role even at photon virtualities of $Q^2 > 5$ GeV^2 [24, 29]. The transition amplitudes for the Roper seem to approach a quark-type behavior only at the highest $Q^2 > 3$ GeV^2 achieved to date. However, even this conclusion is rather uncertain as the displayed models do not include realistic form factor behavior at short distances. For example, there is now evidence that "constituent quarks" have a physical extension and thus require inclusion of form factors [16, 17] to explain the Q^2 dependence of the photo-coupling amplitudes. Dynamical model calculations [38] for the $S_{11}(1650)$ in Fig. 16 show a strong effect of the dressing, even changing sign of the amplitude.

Meson contribution, though large in some cases, cannot explain the transition amplitudes fully. Quarks play an essential role even at large distances. There is also no model calculation available that can explain the measured transition form factors using only dynamically generated resonances. Quenched Lattice QCD calculations, on the other hand, clearly show the existence of excited states. In fact, the lower mass spectrum comes out quite well in these calculations.

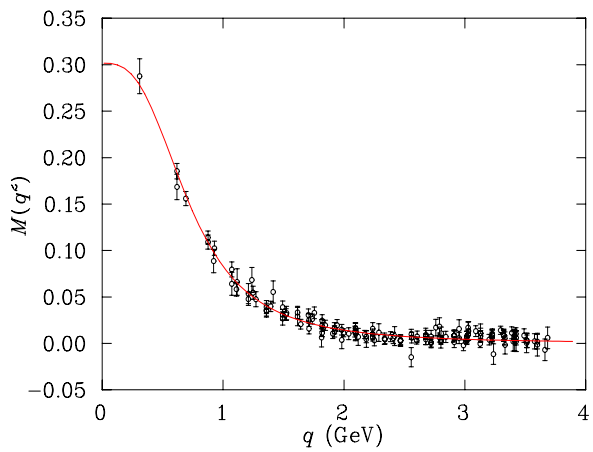

Figure 4: The dressed quark mass vs the momentum transfer from Lattice QCD and the Dyson-Schwinger Equation approach.

In some other cases, e.g. the $S_{11}(1535)$, meson contributions are predicted in the chiral quark model to be much less important than for the $\Delta(1232)$ or the Roper $P_{11}(1440)$ [30], and the empirically measured transition form factors show a harder, quark-like behavior, even at lower Q^2.

For an experimental program to be able to study resonance transitions through the excitation of the quark core, we would need quantitative estimates about the "depth" of the meson cloud, and at what distances the interaction may become dominated by the quark core. To get at least a partial answer we look at the recent calculations within various theoretical frameworks to measure the quark mass M_Q at varying momentum transfer. This

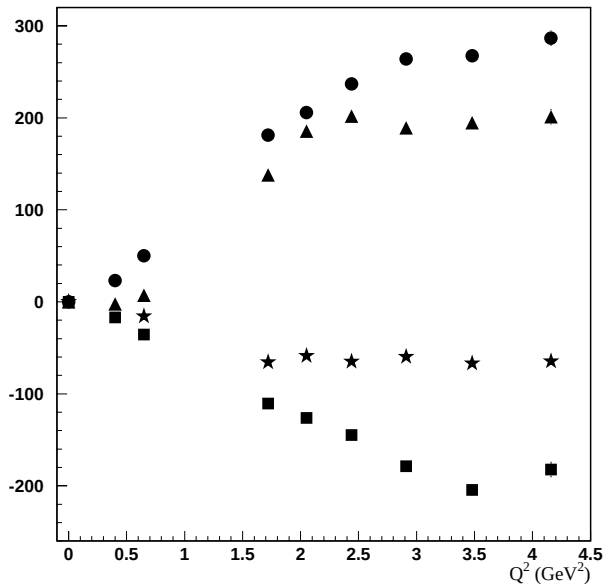

Figure 5: Helicity amplitudes $A_{1/2}(Q^2)$ scaled by $Q^3/1.0$ (GeV^2) for the Roper $P_{11}(1440)$ (triangles), $S_{11}(1535)$ (circles), $D_{13}(1520)$ (squares), and $F_{15}(1680)$ (starts). At the highest Q^2 the dependence is consistent with a flat behavior.

quantity is well defined in Lattice QCD as well as in other approaches, e.g. the Dyson-Schwinger Equation (DSE) approach [12], and in the instanton framework [18]. A representative compilation is presented in Figure 4, which shows the mass of a single quark versus the momentum transfer to that quark. We see that the typical constituent quark mass of 300 MeV/c^2 is approached at $q = 0$ momentum transfer. The mass is reduced slowly with increasing momentum transfer. At $q = 0.9$ GeV/c the quark mass is still 100 MeV/c^2, or 1/3 of the fully "dressed" mass at zero momentum transfer.

Note, that we are dealing here with the momentum transfer to a single quark. For a 3-quark baryon it would appear that on average about 3 times that momentum transfer will be needed, and measurements in the range of $Q^2 = 5 - 10\text{GeV}^2$ should enable us to study the transition from the "dressed" hadron to the valence quark interior. This is just outside the kinematics reach achievable with the current CEBAF machine, but appears to be ideally accessible with the 12 GeV upgrade and the CLAS12 spectrometer. In Figure 5 we show the recent results from the analysis of the CLAS data on $\vec{e}p \rightarrow en\pi^+$ in terms of leading, helicity-conserving helicity $A_{1/2}$ amplitudes to the excitation of the $P_{11}(1440)$, $D_{13}(1520)$, $S_{11}(1535)$, and $F_{15}(1680)$. The amplitudes are multiplied by Q^3, the expected dependence for a point-like coupling to the quarks in the nucleon. We see that the quantity $Q^3 \cdot A_{1/2}(Q^2)$ is consistent with a constant behavior for all resonances and for the highest Q^2, an encouraging sign that "asymptotia" for resonance excitations may be reached with the CEBAF 12 GeV energy upgrade.

2.2 Other directions in N^* studies with CLAS12

2.2.1 GPDs and Baryon Transition Form Factors

An important breakthrough has been the development of the formalism of generalized parton distributions (GPD) [82, 95, 102], which offers a unified framework for accessing the complex structure of hadrons through a variety of exclusive reactions, and promises to yield, for the first time, a truly three-dimensional description of hadrons. Form factors give essential constrains for the GPDs and provide different complementary insights into the unified nucleon structure underlying all exclusive reactions at high momentum transfer in general, and form factors, including nucleon elastic and transition form factors in particular. The role of GPDs in transition form factors has been discussed in Refs. [22], [23] and [109].

Form factors are related to the first moments of GPDs. For elastic scattering from a proton, with $t = -Q^2$, the Dirac and Pauli form factors are written:

$$F_{1p}(t) = \int_{-1}^{1} \sum_q e_q H_p^q(x, \xi, t) dx \qquad F_{2p}(t) = \int_{-1}^{1} \sum_q e_q E_p^q(x, \xi, t) dx$$

where q signifies quark flavors, and for brevity the GPDs are denoted $H^q(x,t) \equiv H^q(x,0,t)$, and $E^q(x,t) \equiv E^q(x,0,t)$. A similar relation holds for neutrons.

Resonance transition form factors access components of the GPDs which are not accessed in elastic scattering. For example, the $N \to \Delta$ form factors, in the large N_c limit are related to isovector components of the GPDs [23] [22];

$$2G_M^* = \int H_M(x,t) dx \propto \int E_M^{(IV)}(x,t) dx$$

Thus, the falloff with Q^2 of the $N \to \Delta$ form factor F_{2p} [114] is shown [109] to be related to the isovector structure of the elastic form factors. This is an area of physics which is undergoing rapid development, and It is expected that analogous GPD relationships can be obtained for the $N \to S_{11}$ and other transitions.

2.2.2 The Q^2 Evolution of N* Structure

Comprehensive data on the evolution of N^* electrocouplings with Q^2 will provide a host of possibilities to examine the internal structure of the nucleon. For example, it will allow us to access the structure of excited nucleon states in terms of the contributing 3-quark configurations at various distance scales. It is well known that the N^* electrocouplings can be related to transition matrix elements between the ground nucleon state and the 3-quark configurations, contributing to N^* wave function as:

$$A_{1/2,3/2} = \sum_i \alpha_i^{\mathrm{N}^*} \underset{i}{<} 3\mathrm{q} \mid \hat{T} \mid \mathrm{g.s.} >, \tag{1}$$

where $\alpha_i^{\mathrm{N}^*}$ represent relative contributions from various 3-quark configurations. $\alpha_i^{\mathrm{N}^*}$ mixing coefficients may be fitted to the data on N^* electrocouplings in a case, if the values of transition matrix elements in Eq.(1) are available.

Analysis of CLAS data on single and double pion electroproduction showed, that with transition matrix elements estimated within the Single Quark Transition Model (SQTM) approach [132], a reasonable fit of the N^* electrocouplings can be achieved. In Fig. 30 we compare the CLAS data on N^* electrocouplings obtained from the analysis of 2π electroproduction [142] with the SQTM fit, shown by the area between the red lines.This example illustrates the capability to access the structure of excited states in terms of the underlying 3q configurations.

The contributions from various 3q configurations are determined by the dynamics of the interactions, which also causes their mixing. Information on mixing coefficients will allow us to establish the relative importance of the one-gluon-exchange (OGE) contribution, and the one-pion-exchange (OPE) contribution [138] at various distances. From this we can establish how mechanisms responsible for quark configuration mixing evolve from the soft regime, which may be affected considerably by OPE, to the partonic regime with gradually increasing OGE contributions.

The proposed approach to access N^* structure is rather flexible and does not rely upon SQTM assumptions. The transition matrix elements in Eq.(1) may be evaluated, using transition operator and contributing 3q configurations taken from any quark model. But the mixing coefficients will be treated as free parameters and fitted to the measured N^* electrocouplings. If a reasonable data description is achieved, the mixing coefficients will give us information on the internal N^* structure. Free variation of mixing coefficients make our approach different from any quark model, where mixing coefficients are fixed, based on assumptions in the specific Hamiltonian used in the model. Instead, our approach represent a phenomenological way to access N^* structure from the analysis of the N^* electrocouplings, and is not restricted by any particular assumption on the Hamiltonian. The information on N^* structure derived in phenomenological analysis may be used as input to determine the underlying Hamiltonian. In particular, it will be most interesting to try to obtain access to the confinement potential. Since the transition matrix elements in Eq.(1) are determined by parameters of the confinement potential, we may fit them simultaneously with the mixing coefficients to the N^* electrocouplings. The information obtained from these fits may be directly confronted with lattice predictions for the confinement potential. In this way we may check fundamental QCD expectations on the binding mechanisms that is responsible for the formation of baryons.

To provide access to the N^* Hamiltonian, comprehensive data on N^* electrocouplings in a wide Q^2 range covered by *CLAS12* are needed.

2.3 Expected data base and analysis approaches

This proposal is aims to measure the evolution of the transition form factors to the excited nucleon quantum states over a range of Q^2 from 4.0 to 14 GeV^2. We expect that there will be a contemporaneous evolution in the theoretical tools for describing the evolution from the long range to the short range structure of these nucleon quantum states.

We propose to determine Q^2-evolution of electrocouplings for N^* states with masses less

than 3 GeV, including possible new baryon states, from the analysis of two major exclusive channels: $ep \to ep\pi^0$, $ep \to en\pi^+$, and $ep \to ep\pi^+\pi^-$ ($ep \to ep\eta$ will be measured as well). All channels will be measured simultaneously with *CLAS12*. An extensive data base for N^* studies will be created from the proposed measurements.

For the π^+n and π^0p channels the following observables will be measured in each W and Q^2 bin:

- complete azimuthal and polar angular distributions for π^+, π^0
- polarized beam asymmetries A_e

Data on $\pi^-\pi^+p$ production for each W and Q^2 bin will consist of:

- $\pi^-\pi^+$, π^+p, π^-p invariant mass distributions
- π^+, π^-, p cm-angular distributions
- 3 distributions over angles between two planes, composed by two pairs of 3-momenta of the final hadron for 3 various choices of hadron pairs

Overall 18 observables in each bin will be available to evaluate the N^* electrocouplings in a combined analysis of single and double pion production.

In the first stage, the N^* electrocouplings will be extracted in fits to the 1π and 2π channels combined, but neglecting their mutual couplings. Phenomenological approaches have been developed for that purpose [36, 142]. These two approaches will be applied separately for the two channels, however all data will be fitted with a common set of N^* electrocouplings. Successful fit of all observables in two major exclusive channels will provide initial information on N^* electrocouplings. A final evaluation of N^* electrocouplings will be carried out within the framework of the most advanced coupled channel approach, which is now under development within the Excited Baryon Analysis Center (EBAC) at the JLab Theory Center. This approach is discussed in detail in Sect. 4.2-4.5. From such a procedure we expect reliable results on N^* electrocouplings. Moreover, the result of this analysis will have strong impact on N^* studies in all other exclusive channels. Single and double pion production, being major contributors, should affect considerably all other exclusive reactions through channel couplings.

The next three sections describe in more detail the basic motivation for for studying the properties of baryon resonances over a large range of Q^2. Section 2 deals with single meson electroproduction, which historically has been the subject of most in-depth work. Section 3 then discusses two meson electroproduction, and its potential for augmenting single meson production as an equal partner in the expanded experimental program. Section 4 then explores the most vital question of what we will do with this plethera of data forthcoming from the experimental program. That is, how we will put it all together in a coupled channel approach to extract the photo-couplings for the individual N* resonances.

3 Single Pion Exclusive Channels

A large portion of the nuclear physics community enthusiastically started to investigate baryon resonances as new optimized detector systems with large solid angle and momentum coverage like CLAS and new high-intensity continuous electron beams like at JLab became available. The high versatility of the provided electromagnetic probes that have negligible initial state interactions have produced intriguing results ever since. It was realized that isoscalar or isovector, and the electric, magnetic or longitudinal character of the coupling to hadronic matter probe different aspects of the strong interaction. However, the desired versatility of the electromagnetic probe comes with the complication that it mixes all the different coupling amplitudes simultaneously into the measured cross sections. A way out has been successfully demonstrated in the case of the $N \to \Delta(1232)$ transition, where the small resonant electric R_{EM} and scalar quadrupole R_{SM} amplitudes could be extracted with respect to the dominant magnetic dipole amplitude with absolute systematic uncertainties of typically 0.5% [13, 80, 84], see Fig. 2 at intermediate momentum transfers $0.2\,GeV^2 \leq Q^2 \leq 1.0\,GeV^2$. To obtain such precision results for the extraction of isolated resonance parameters, additional isospin channels and polarization observables had been measured to disentangle the individual resonant and non-resonant coupling amplitudes [77, 86, 89]. A similar precision of $R_{EM} \approx -2.5\% \pm 0.5\%$ [14] was achieved in photo-production for an even more complete set of observables, and the fundamental approach of how to peform a complete experiments in pseudoscalar photo-production is described in [90].

Several very recent [97, 110] results from e1-6 run period [1] at an electron beam energy of $5.75\,GeV$ are reshaping the understanding of nucleons, and nucleon excitations and are presenting new opportunities in a way that demands an extension of this successful program based on the experience and knowledge already gained at JLab.

One of these results is the extension of the $N \to \Delta(1232)$ transition form factors to higher momentum transfers [110], where pQCD predicts in the high Q^2 limit, by neglecting higher twist contributions, a R_{EM} of $+1$, a Q^2 independent R_{SM}, and a $1/Q^4$ fall-off of G_M^*. The experimental results, now available up to $6\,GeV^2$, as shown in Fig. 2, reveal no indication of the predicted behavior in any of the three cases, but rather follow the same overall trend as established in the non-perturbative regime. This is particularly striking in the case of the magnetic $N \to \Delta(1232)$ transition form factor G_M^*, where the simple constituent counting rule would demand the $1/Q^4$ dipole form; as well as in the case of the R_{EM}, that is defined by the helicity conserving amplitude $A_{1/2}$ and the helicity non-conserving amplitude $A_{3/2}$,

$$R_{EM} = \frac{A_{\frac{1}{2}} - \frac{1}{\sqrt{3}} A_{\frac{3}{2}}}{A_{\frac{1}{2}} + \sqrt{3} A_{\frac{3}{2}}} \tag{2}$$

where the simple argument of helicity conservation at high momentum transfers demands $A_{3/2} \ll A_{1/2}$, which directly leads to the prediction of $R_{EM} = +1$.

[1] Proposal E99-107: *"N^* Excitations at High Q^2 in the $p\pi^0$, $p\eta$, and $n\pi^+$ Channels"*

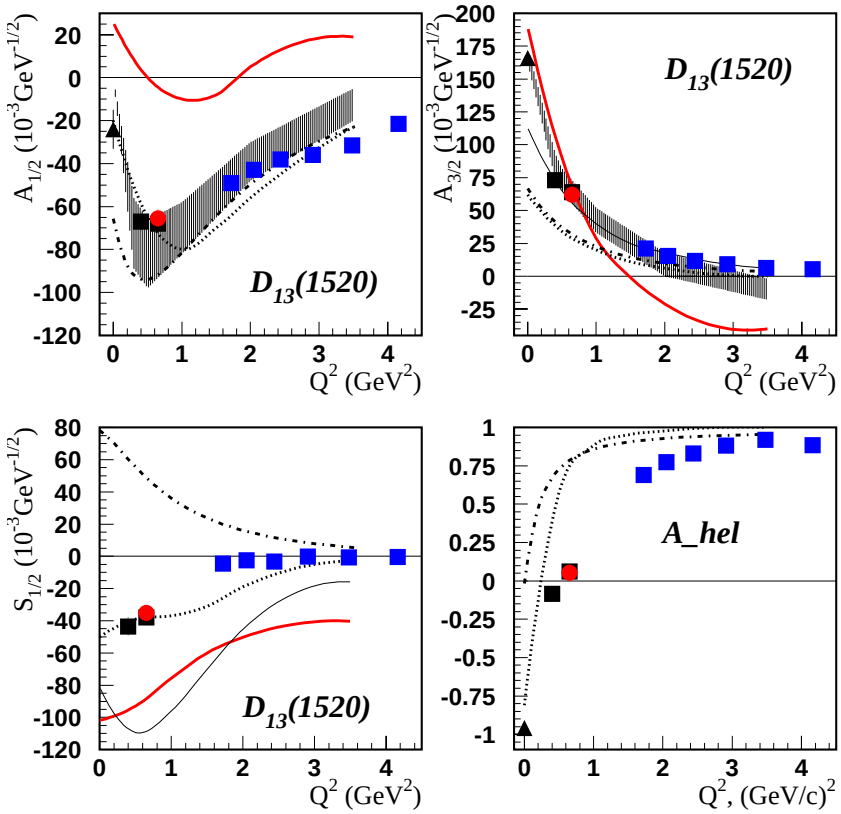

Figure 6: Helicity amplitudes for $\gamma^* p \to D_{13}(1520)$ transition in $10^{-3}\,GeV^{-1/2}$ and the helicity asymmetry as defined in the text. The data points are CLAS results [77, 84–86]: filled black squares from the analysis of the π electro-production data [36], filled red circles from the combined analysis of π and 2π electro-production data [52], filled blue squares from the analysis of preliminary π^+ electro-production data [97], filled black triangle from the PDG estimate at the real-photon point [99], and hatched area based on Bonn, DESY, NINA, and JLab η electro-production data [132]. The curves are based on the following calculations: solid dash-dotted curves on q^3 $q\bar{q}$-cloud [72], and all other curves are further quark model calculations [46, 71, 96, 112].

So, the remaining question is, at which Q^2 should helicity conservation as well as a pQCD description start to dominate. Perhaps a momentum transfer of $6\,GeV^2$ is still not large enough. We may attempt to deduce the answer from the lattice calculation (LQCD) [62] of the quark mass M as function of the quark propagator momentum q and the fact that helicity is conserved when the momentum of the hadron is large compared to its mass $q \gg M$. In contrast to the momentum transfer that has to be shared between all three quarks, the angular momentum transfer in resonance excitations can either involve several quarks and more complicated configurations or in principle also only one quark. The quark mass function in Fig. 4 gives at $q = 2\,GeV$ a quark mass of the order of $15\,MeV$, which roughly corresponds to a momentum transfer of $4\,GeV^2$ for the simplest assumption that only

a single quark absorbs the angular momentum introduced by the virtual photon. Here the condition for helicity conservation would definitely be fulfilled, but it would gradually break down for $q \leq 1\,GeV$, where quark mass steeply increases with decreasing quark momentum. These arguments lead to the prediction that for resonances that conserve angular momentum on the single quark level the helicity conserving amplitude $A_{1/2}$ should dominate the helicity non-conserving amplitude $A_{3/2}$ at $Q^2 \geq 1\,GeV^2$. This predicted behavior is indeed clearly visible for the $D_{13}(1520)$ helicity amplitudes and helicity asymmetry

$$A_{hel} = \frac{A^2_{\frac{1}{2}} - A^2_{\frac{3}{2}}}{A^2_{\frac{1}{2}} + A^2_{\frac{3}{2}}} \tag{3}$$

in Fig. 6 [97]. The tremendous difference between the results for A_{hel} in the $D_{13}(1520)$ and R_{EM} in the $\Delta(1232)$, both based on the same fundamental principle of helicity conservation, marks the unexplored range between the simplest and probably most involved momentum transfer dynamics that can be studied in the proposed experiment.

Interestingly, it has been suggested [98] that the $N \to \Delta$ may really not be the easiest place to search for the onset of pQCD, since there may be an accidental cancellation between the pQCD amplitudes involving the symmetric and antisymmetric part of the proton quark distribution amplitude coupling to the purely symmetric distribution amplitude of the Δ.

It is therefore not only important to extend these measurements of the $N \to \Delta(1232)$ transition form factors to even higher momentum transfers, but also to investigate the Q^2 evolution of exclusive transition form factors to other higher lying resonances.

The most recent results for the reaction $\gamma^* p \to n\pi^+$ [97], as already referred to in Figs. 3 and 6 have been obtained in an analog procedure to the one proposed here and described in chapter 6 and 7. Since especially the Roper(1440) resonance parameters have always been notoriously hard to extract, the variety of different theoretical approaches to describe them is extensive and includes q^3, $q^3 + q\bar{q}$ cloud, and $q^3 + g$ hybrid quark models as well as dynamical generating and $N + \sigma$ molecule models, see Fig. 3. The presented helicity coupling amplitudes for the higher lying resonances $P_{11}(1440)$, $S_{11}(1535)$, $D_{13}(1520)$, and $F_{15}(1680)$, that have been extracted up to $4.5\,GeV^2$, illustrate the quality of the new results and show that none of the present model calculations is able to describe neither magnitude nor Q^2 trend of these helicity amplitudes of all four resonances consistently.

Still maybe the most interesting new result is that here, as well as in the two-pion production channel, many resonances are easier to isolate at higher Q^2 than at or close to the real photon point. Fig. 7 demonstrates how dramatically the resonance behavior of the real and the imaginary part of the resonant multipole amplitudes are enhanced at higher Q^2, where E_{0+} is the dominating resonant multipole of the $S_{11}(1535)$ and M_{1-} of the $P_{11}(1440)$. The shown resonant multipole amplitudes at the real photon point reflect the difficulties of isolating the Roper resonance, which even does not produce a peak in the inclusive cross section (see Fig. 18), and the $S_{11}(1535)$, which had to be investigated in the η production channel to allow a clean separation from neighboring resonances and background contributions.

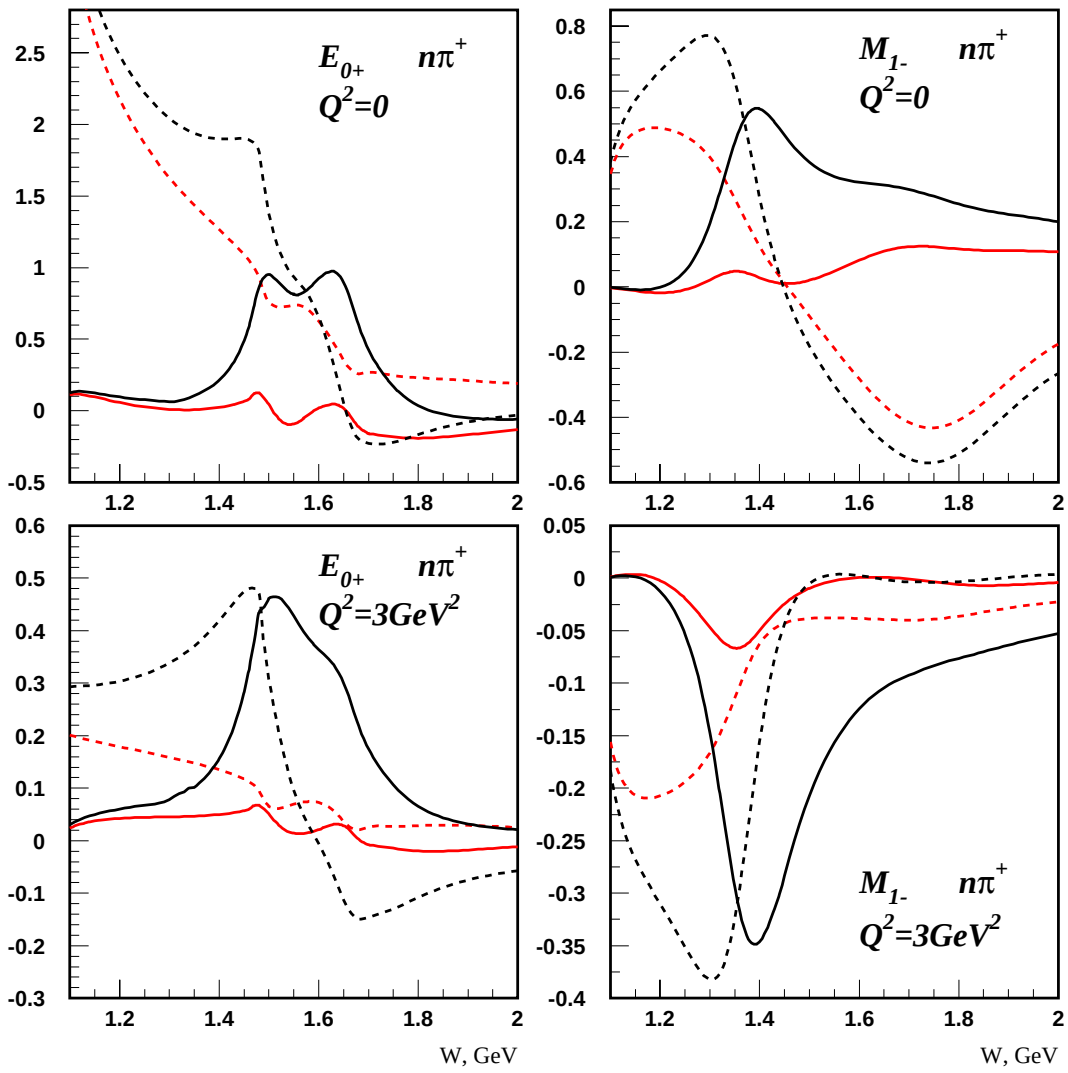

Figure 7: Pion production multipole amplitude M_{1-} (E_{0+}) that contributes dominantly to the $P_{11}(1440)$ ($S_{11}(1535)$) resonance for $Q^2 = 0$ (upper panels) and $Q^2 = 3\,GeV^2$ (lower panels). Black curves: total amplitudes, red curves: background, solid curves: imaginary part, and dashed curves real part of the amplitudes.

Since many resonances become more visible and easier to investigate at higher Q^2, we not only propose to extend the study of the shown $\Delta(1232)$, $P_{11}(1440)$, $S_{11}(1535)$, $D_{13}(1520)$, and $F_{15}(1680)$ resonances up to $Q^2 = 12\,GeV^2$, but also propose to extend the scope to identify further resonances to the full invariant mass region $1.0\,GeV \leq W \leq 4.5\,GeV$. This experiment should at least enable us to investigate the peak structure beyond the $F_{15}(1680)$ resonance, as seen in the inclusive cross section data set in Fig. 18, and has the potential to find further resonances, which as the Roper(1440) do not exhibit any peak structure in any of the Q^2 panels of Fig. 18.

4 Double Charged Pion Exclusive Channel

The studies of double pion production by real and virtual photons [115–123, 125–128] clearly demonstrate the capability of this exclusive channel to provide important information on N^* electrocouplings and hadronic decay parameters for most excited proton states. The information on N^* parameters extracted from 2π electroproduction is complementary to that obtained in the single pion channel. While the single pion channel is sensitive mostly to N^* in the mass range less than 1.7 GeV [19], the two-pion channel exhibits the contributions from both low lying (M<1.6 GeV) and high lying (1.6<M<3.0 GeV) N^* states. Most of the high lying excited proton states have substantial, even dominant two-pion decays [129]. Thus, two-pion channel offers a promising way to obtain comprehensive data on Q^2-evolution of electromagnetic form factors for most excited proton states.

The information from double pion exclusive channels is necessary to access electrocouplings and hadronic parameters of the $S_{31}(1620)$, $D_{13}(1700)$, and $D_{33}(1700)$ states of the $[70,1^-]$-plet and almost all states which belong to the $[56,2^+]$-plet. Various quark model predictions [71, 130, 131] are available for the description of N^* electrocouplings, including high lying states. They are complemented by general schemes based on underlying driving symmetries, which allow us to relate N^* electrocouplings within particular symmetry multiplets [112, 132, 133]. These approaches provide good bases for developing a physics analysis framework for relating new data on N^* electrocouplings in an unexplored area of Q^2 at distances corresponded to the transition from soft to partonic regimes. In particular we may study the relative contributions from the meson cloud, quark clusterization (di-quarks) and the 3-quark core at various distance scales[31, 134, 135]. Comprehensive information on N^* electrocouplings may allow us to investigate the relative contributions from OGE and OPE mechanisms at various distance scales from soft to partonic regimes [138]. Another interesting opportunity may be the possible observation of the leading symmetry evolution for quark binding forces. Such evolution is actually required by chiral symmetry restoration for the entire spectrum of nucleon excitation at some still undetermined high Q^2, for which the momentum transfer for a single constituent is significantly larger than the basic QCD scale Λ^2_{QCD} [139].

Double pion electroproduction offers the most promising way to study N^*s in the mass range from 2.0 to 3.0 GeV. According to the data from experiments with hadronic probes [129] as well as quark model expectations [140], these heaviest N^* should mostly manifest theirselves in two-pion exclusive channels. The studies of these particular N^*s will allow the investigation of possible chiral symmetry restoration for highly excited nucleon states, predicted in [139, 141]. Moreover, the quark models dealing with various effective constituents (3-quarks or quark di-quark configurations) [71, 130, 136, 137] predict still unobserved, so-called "missing", baryon states. Such resonances are decoupled from the single-pion decay channel and likely may be observed in two-pion electroproduction.

The heaviest N^*s, accessible primarily in two-pion electroproduction, have the largest angular momenta and correspond to maximal radial excitations. Therefore, their studies will shed light on evolution of N^* binding forces with orbital momenta and radial quantum

numbers.

Recent lattice studies of 3-quark confinement potentials [7] show that the energy gap separating the ground state potential and the potential built on the first excited flux tube state, is of order 1.0 GeV. This lattice result explained the success of the quark models in describing the nucleon resonances with excitation energy lower than 1.0 GeV, neglecting glue-gluon degrees of freedom. Constituent quark excitation energies are on the order of hundreds of MeV, which is much smaller, than the energy corresponding to excitation of flux tubes. On the other hand, the structure of heavy resonances with masses above 2.0 GeV may be considerably affected by flux tube excitations. According to Ref. [7] such hybrid configurations represent collective excitation of all three flux tubes and all three quarks. Such highly collective excitations should posses very peculiar features for their electromagnetic form factor behavior. Furthermore, these collective hybrids would likely decay with multi-pion emission. Therefore, particular features in the electromagnetic form factor behavior in a wide Q^2 involving the two-pion channel offers a promising way to discover hybrid states at masses above 2 GeV.

5 Combined Studies of Various Exclusive Channels

Individual 1π and 2π channel analyses [50, 51, 142] of the CLAS data with a 6.0 GeV beam already have provided information on the Q^2 evolution of N^* electrocouplings. For the first time data on N^* electrocouplings were obtained in an extremely wide range of Q^2 up to about $5\,GeV^2$. Electrocouplings for $D_{13}(1520)$ and $F_{15}(1685)$ states extracted from the CLAS data are shown on Fig. 8 and Fig. 9. In the short term 2π electro-production cross-sections from the e1-6 run will be available in the entire N^* excitation region at photon virtualities from 1.6 to 5.0 GeV^2.

The CLAS12 detector will offer a unique opportunity to study N^* in all exclusive channels simultaneously at high Q^2. Experience in N^* studies clearly demonstrates the importance of the combined analysis of various exclusive channels to obtain reliable information about resonance electro-couplings and hadronic decay parameters. In the proposed experiments we are focusing on combined studies 1π and 2π electro-production off protons.

The combined analysis of 1π and 2π exclusive electro-production off protons is absolutely necessary for the reliable evaluation of N^* electromagnetic form factors. The credible separation between resonant and non-resonant mechanisms represents a challenging problem for any approach used for extraction of the N^* electro-couplings. The current status of understanding strong interactions in the non-perturbative domain, makes it is impossible to estimated the non-resonant part based on fundamental theory. Also phenomenological analyses, even for the data of the highest quality, do not allow us to disentangle the resonant and non-resonant parts in model a independent way, especially when their contributions are comparable.

Such a situation is most common in N^* analysis at invariant masses of the final hadronic system W>1.5 GeV. An effective way to insure credible separation between resonant and non-resonant mechanisms may indeed be the combined analysis of 1π and 2π channels which account for the major part of the total virtual photon cross-section in the N^* excitation region. Furthermore, the two channels have entirely different non-resonant mechanisms. Therefore, the successful description of all observables measured in 1π and 2π electro-production off protons with a common set of N^* electro-couplings and hadronic parameters would provide reliable separation between the resonant and non-resonant contributions in both exclusive channels. A successful description of all observables in 1π and 2π channels with a common set of N^* electro-couplings and hadronic parameters was achieved in a combined analysis of CLAS data at $Q^2 = 0.65\,GeV^2$ [52], providing strong support for phenomenological approaches [50, 51, 142] in CLAS data analysis. However, in this combined fit, particular models for analysis of 1π and 2π data were applied separately and independently. Currently, an effort coordinated by EBAC is underway, which will be capable of taking into account interactions between these two major electro-production channels within the framework of a rigorous coupled channel formalism (Chapt. 5.2-5.5)

Using electromagnetic beams, a number of channels can and must be explored. The excited states of the nucleon and Δ may be examined in channels such as $N\pi$, $N\pi\pi$, YK, $N\eta$, $N\omega$ and $N\eta'$. The final states that include the ground state hyperons and kaons provide

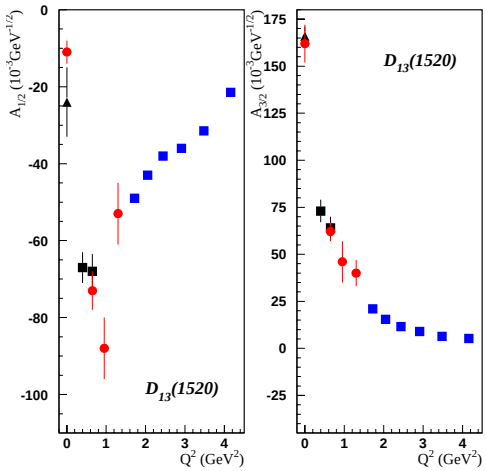

Figure 8: Photo- and electro-couplings for $D_{13}(1520)$ obtained from analysis of CLAS data on 1π, 2π electro-production. The results from 1π data analysis are shown by blue squares (preliminary analysis of e1-6 run) and by black squares [36]. The results from the 2π channel are shown by red circles [52, 142], while PDG values at the photon point are shown by black triangles.

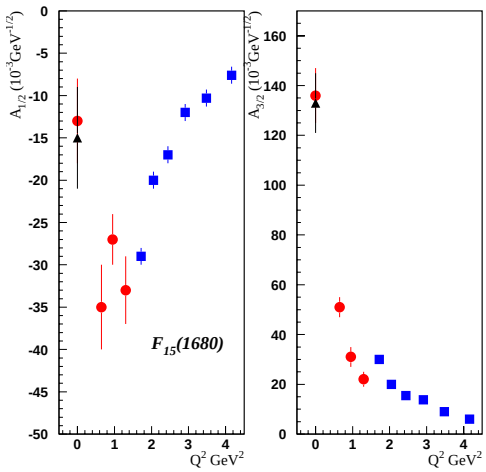

Figure 9: Photo- and electro-couplings for $F_{15}(1685)$. The symbols for experimental points are the same as on Fig. 8.

information on an important part of the QCD puzzle: how do nonstrange baryons couple to states with strangeness. It must also be emphasized that verifying the predicted multiplet structure of the excited baryons will require that the strange members of the multiplets be

identified. This means that channels such as NKK, $YK\pi$, $YK\eta$ and ΞKK must also be exploited.

The Jlab $12\,GeV$ upgrade and CLAS12 are uniquely suited to carry out a cohesive program of exclusive measurements extending the momentum transfers toward the region where pQCD effects become visible. In contrast to conventional experiments employing magnetic spectrometers that focus on specific excitations at specific kinematics, CLAS12 allows the simultaneous measurement of angular distributions over a wide range of W and Q^2 for many exclusive channels, including not only single-meson production processes, such as π, η, and K, but also multi-meson final states.

5.1 Coupled-Channel Analysis

One of the primary activities of the N* program at JLab is to develop a sound basis for the reliable extraction of the resonance electro-production amplitudes. The required concerted theoretical effort has already begun with the formation of the Excited Baryon Analysis Center (EBAC). It is well recognized that that this effort will require a coupled channel approach involving all final state channels, including one and two meson production.

The necessity for performing a coupled-channel analysis of the data obtained from these and other experiments stems essentially from the unitarity condition. For the specific case of pion photo-production, the effect of the unitarity condition on the analysis that can be carried is illustrated in Fig. 10. In this figure, the dashed lines are the imaginary part of the non-resonant amplitudes obtained if the unitarity condition is ignored, while the solid curves just above or below the dashed lines result when this condition is properly taken into account.

5.2 Development of Dynamical Coupled-Channel Analysis at EBAC

The Excited Baryon Analysis Center (EBAC) was established at Jefferson Laboratory (JLab) in January, 2006. The objective is to develop theoretical approaches to *extract* and also *interpret* the nucleon resonance (N^*) parameters by using the very extensive JLab data of electromagnetic production of pseudoscalar mesons, π, η, K, and also two pions.

The team members are Bruno Julia-Diaz (University of Barcelona), T.-S. Harry Lee (Argonne National Laboratory), Akihiko Matsuyama (Shizuoka University), Mark Paris (EBAC), and Toru Sato (Osaka University). Harry Lee, serving as the Leading Investigator of EBAC, is coordinating the effort. All members of this team have extensive experiences in performing large-scale numerical calculations, as seen, for example, in their publications[32–35].

The starting point of this effort is the Argonne-Osaka-Shizuoka (AOS) model[31] which has been developed in the past three years by three members of this team. Most of the computation codes needed for performing dynamical coupled-channel calculations with γN, πN, ηN, $\pi\pi N$ ($\pi\Delta$, ρN, σN) channels have been developed. As illustrated in Fig.11, the current computation codes for the AOS model already can give a reasonable account of the

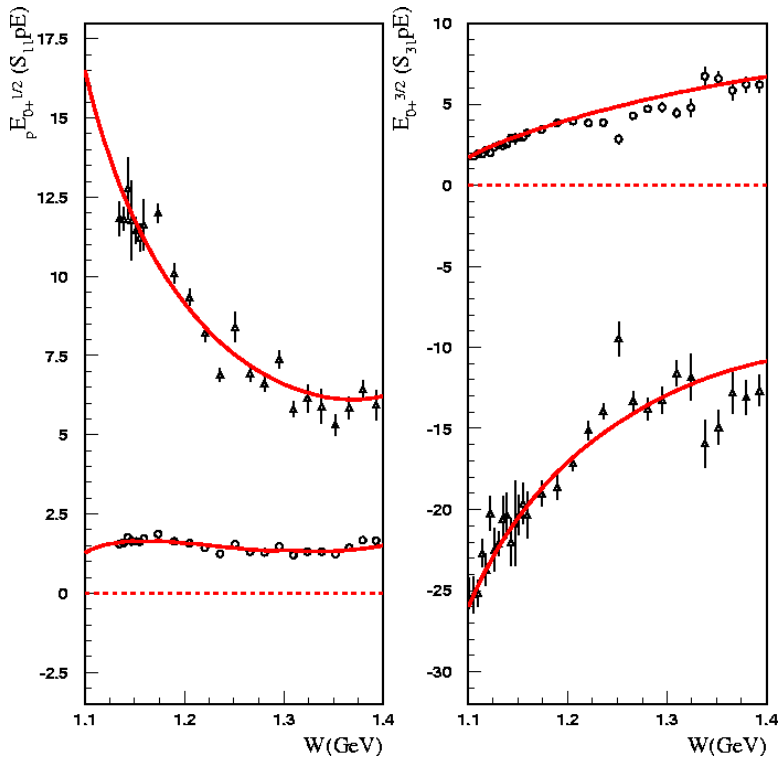

Figure 10: The effect of the unitarity condition on the E_{0+} amplitudes from the S_{11} (left panel) and S_{31} (right panel) non-resonant partial waves. In each case, the imaginary part of the amplitude is given by the dashed line when the unitarity condition is ignored. When this condition is properly applied, the results agree very well with the extracted imaginary parts of the amplitudes (open circles).

two pion photo-production data from CLAS. However the parameters of the model have not been optimally determined. Thus, the first task of this project is to bring the computation codes of AOS model to production stage for extracting N^* parameters from JLab data. We then will implement the input from hadron structure calculations, such as those from constituent quark models at the present time and Lattice QCD in the near future, to interpret the extracted N^* form factors.

Here we will only describe the plan for carrying out the first part of this project. The main task is to calculate the meson-baryon amplitudes defined by

$$T_{MB,M'B'}(k,k',E) \;=\; t_{MB,M'B'}(k,k',E) + t^R_{MB,M'B'}(k,k',E)\,, \tag{4}$$

where $MB = \gamma N, \pi N, \eta N, \pi\Delta, \rho N, \sigma N$. The non-resonant amplitudes $t_{MB,M'B'}(E)$ in Eq.(4) are obtained from solving the following coupled-channel equations

$$\begin{aligned} t_{MB,M'B'}(\vec{k},\vec{k'},E) \;&=\; \hat{V}_{MB,M'B'}(\vec{k},\vec{k'},E) \\ &+ \sum_{M''B''} \int d\vec{k''} \hat{V}_{MB,M''B''}(\vec{k},\vec{k''},E) G_{M''B''}(\vec{k''},E) t_{M''B'',MB}(\vec{k''},\vec{k'},E)\,, \end{aligned}$$

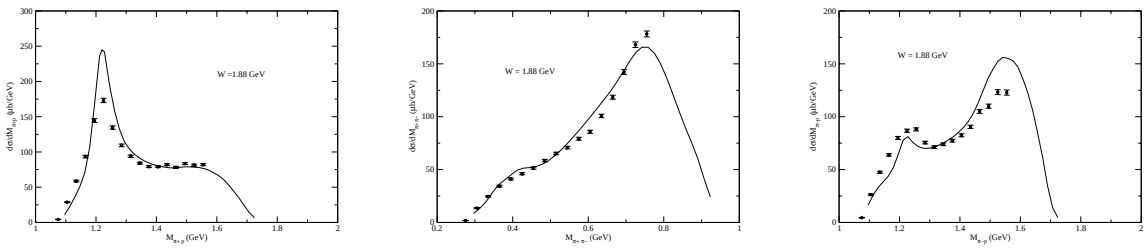

Figure 11: The differential cross sections of of $\gamma p \to \pi^+\pi^- p$ reaction with respect to the invariant mass M_{π^+p} (left), $M_{\pi^+\pi^-}$ (center), and M_{π^-p} (right) at W=1.88 GeV. The data are from CLAS.

(5)

where $G_{MB}(k,E)$ is the meson-baryon propagator, and the driving term is

$$\hat{V}_{MB,M'B'}(\vec{k},\vec{k'},E) = v_{MB,M'B'}(\vec{k},\vec{k'}) + Z^{(E)}_{MB,M'B'}(\vec{k},\vec{k'},E)\,. \tag{6}$$

The matrix elements $v_{MB,M'B'}(\vec{k},\vec{k'})$ of the non-resonant interactions, defined by the meson-exchange mechanisms, are finite and integrable. The complication in solving Eq.(5) is from the one-particle-exchange term $Z^{(E)}_{MB,M'B'}(\vec{k},\vec{k'},E)$ which diverges logarithmically in the moon-shape regions illustrated in left side of Fig.12. The rapidly varying structure of their matrix elements, as illustrated in the right side of Fig.12, needs to be carefully accounted for in solving Eq.(5). In particular, its imaginary part (dashed line) has a discontinuous structure and is non-zero only in a narrow region.

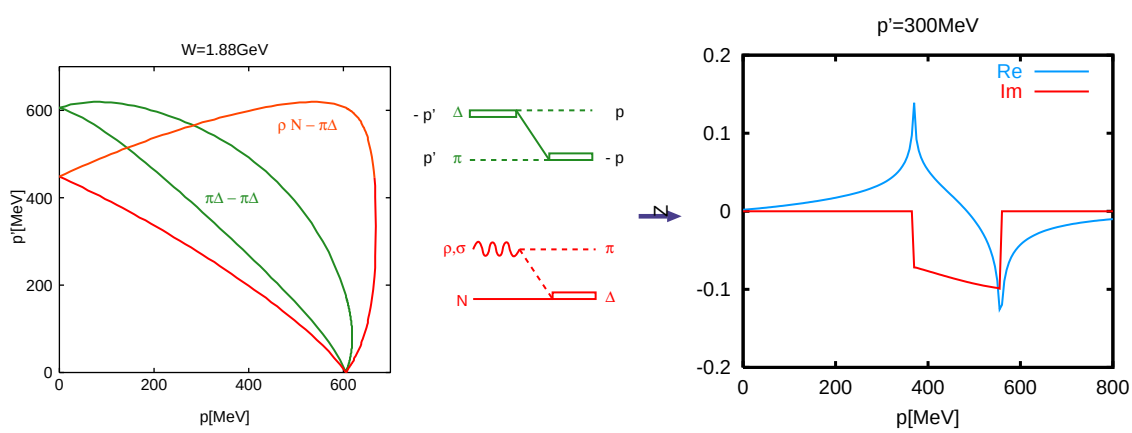

Figure 12: Left side : Singularity structure of the driving terms $Z^{(E)}_{\pi\Delta,\pi\Delta}$ and $Z^{(E)}_{\rho N,\pi\Delta}$ at W=1.88 GeV. Right side: The half-off-shell matrix element of $Z^{(E)}_{\pi\Delta,\pi\Delta}(p,p',W)$ with $p' =$ 300 MeV/c and W=1.88 GeV.

Hadronic dressing for N^* electromagnetic verticies and propagators, due to interaction with open MB channels are schematically presented in Fig. 13, Fig. 14.

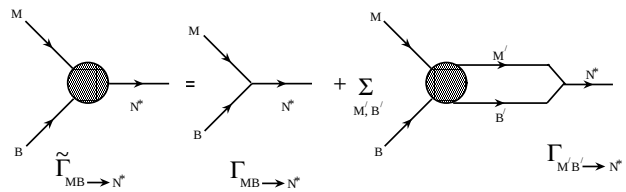

Figure 13: N^* electromagnetic verticies: bare (points) and dressed due to coupled channel effects (blobs).

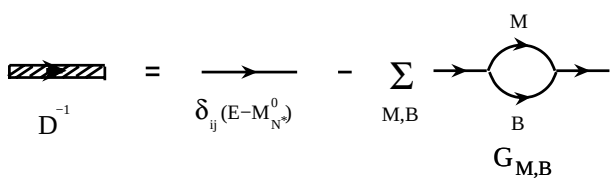

Figure 14: N^* propagators: bare (thin lines) and dressed due to coupled channel effects (thick lines).

The resonant term of Eq.(4) is

$$t^R_{MB,M'B'}(k,k'E) = \sum_{N_i^*,N_j^*} \bar{\Gamma}_{MB\to N_i^*}(k',E)[D(E)]_{i,j}\bar{\Gamma}_{N_j^*\to M'B'}(k,E)\,, \tag{7}$$

with the dressed vertex interaction defined by

$$\bar{\Gamma}_{MB\to N^*}(E,k) = \Gamma_{MB\to N^*}(k) + \sum_{M'B'}\int d\vec{k'} t_{MB,M'B'}(\vec{k},\vec{k'},E)G_{MB}(k',E)\Gamma_{M'B'\to N^*}(k')\,, \tag{8}$$

and the N^* propagator by

$$[D(E)^{-1}]_{i,j} = (E - M^0_{N_i^*})\delta_{i,j} - \sum_{MB}\int k^2 dk \Gamma_{N_i^*\to MB}(k)G_{MB}(k,E)\bar{\Gamma}_{MB\to N_j^*}(E,k)\,. \tag{9}$$

where $M^0_{N^*}$ and $\Gamma_{M'B'\to N^*}(k)$ are the bare mass and bare vertex the N^* state, respectively.

Once the $MB \to M'B'$ amplitudes are obtained, we can calculate the matrix elements of the two-pion photo- and electro-production

$$\begin{aligned} T_{\pi\pi N,\gamma N}(E) &= v_{\pi\pi N,\gamma N} + [v_{\pi\pi N,\pi N}G_{\pi N}(E)T_{\pi N,\gamma N}] \\ &\quad +\Gamma^\dagger_{\Delta\to\pi N}G_{\pi\Delta}(E)T_{\pi\Delta,\gamma N}(E) \\ &\quad +h^\dagger_{\rho\to\pi\pi}G_{\rho N}(E)T_{\rho N,\gamma N} \\ &\quad +h^\dagger_{\sigma\to\pi\pi}G_{\sigma N}(E)T_{\sigma N,\gamma N} \end{aligned} \tag{10}$$

where $v_{\pi\pi N,\pi N}$ and $v_{\pi\pi N,\gamma N}$ are the direct non-resonant production amplitudes. $v_{\pi\pi N,\pi N}$, $v_{\pi\pi N,\gamma N}$ are calculated from tree-diagrams of effective Lagrangians.

The computer programs for calculating the above equations have been developed in Ref.[31]. In particular, a numerical method based on a spline-function expansion for dealing with the two-pion channels has been developed and well tested. The unique capability of this method is demonstrated in Fig.15 where the effects due to $\pi\pi N$ cuts, which are neglected in all recent calculations, are shown to be important in interpreting the two-pion photo-production data.

To proceed, we need to first determine the parameters associated with the non-resonant amplitude $t_{MB,M'B'}$ of Eq.(4) such that the N^* parameters of the resonant term $t^R_{MB,M'B'}$ can be extracted from fitting the data of meson production reaction. In the following sections, we describe how we will carry out this research project.

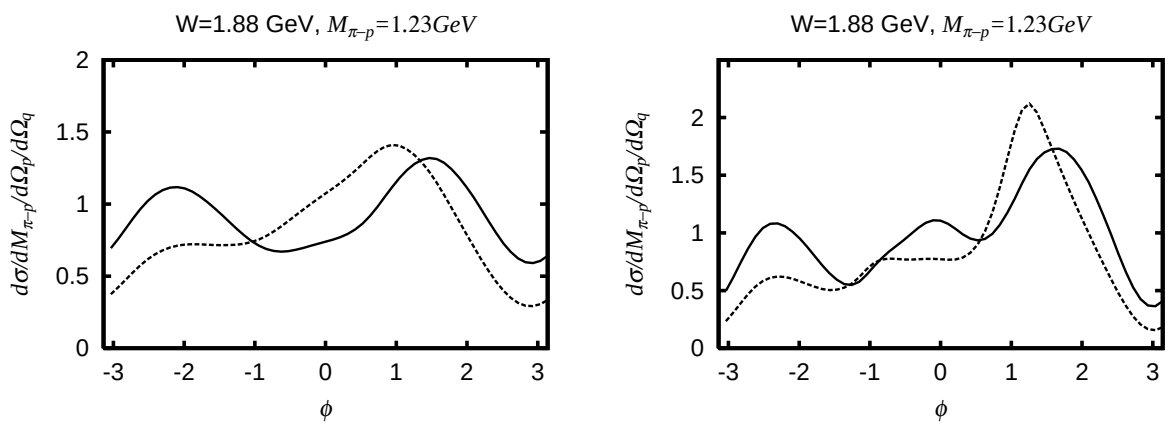

Figure 15: Differential cross sections of $\gamma p \to \pi^+\pi^- p$ at W=1.88 GeV. The dotted curves are obtained when $\pi\pi N$ cut effects in $Z(E)_{MB,M'B'}$ of Eq. 6 are neglected. The outgoing π^+ momentum, is $\vec{p}$ and the relative momentum between π^- and p is $\vec{q}$. ϕ is the azimuthal angle of $\vec{q}$. The results are for $M_{\pi^- p} = 1.23$ GeV, $cos\theta_p = 0.183$, $\phi_p = -3.1$ rad. The left (right) panel is for $cos\theta_q = -0.96(-0.525)$

5.3 Fit to πN data

The first step is to determine the parameters of the hadronic non-resonant interaction $v_{MB,M'B'}$ of Eq.(6), with $MB = \pi N, \eta N, \pi\Delta, \rho N, \sigma N$. This will be done by fitting the πN elastic scattering data.

We will perform the fits in three stages. In the first stage, the resonant amplitude $t^R_{\pi N,\pi N}$ of Eq.(4) will be generated from the resonance parameters listed by Particle Data Group (PDG) using the procedures explained in Ref.[31]. Furthermore the one-particle-exchange term $V^{(E)}_{MB,M'B'}$ can be neglected in solving coupled-channel equation Eq.(5) since its effects

on $\pi N \to \pi N$ elastic scattering amplitudes are known[31] to be weak. Even with these two simplifications, the χ^2-fit to πN data requires fast and efficient calculations of Eq.(5). Casting the codes of Ref.[31] into a form suitable for parallel computations is essential. The necessary starting computation resource has already been obtained from NERSC of U.S. Department of Energy. An application to Spain's Barcelona Supercomputing Center will be submitted to get additional computation power.

Once the parameters, coupling constants and ranges of form factors, of $v_{MB,M'B'}$ are determined, our procedure in the next stage is to allow the resonance parameters to vary in the fits. Here we will work with Richard Arndt, the leading expert in πN amplitude analyses, to narrow down the dressed N^* parameters associated with the strong decay channels. In particular, we need to clarify the questions concerning the decomposition of $\pi\pi N$ into quasi-two particle channels $\pi\Delta, \rho N, \sigma N$ in their empirical partial-wave analyses.

In the third stage, we need to include the particle-exchange term $Z^{(E)}_{MB,M'B'}$ of Eq.(6) in the fits to tune the parameters. Here we will use the code based on the spline-function expansion, which has also been developed and well tested in Ref.[31].

We expect to complete the fits to πN data by the end of 2006.

5.4 Extraction of $\gamma N \to N^*$ Form Factors

Once the πN data are fitted, most of the strong verticies in the non-resonant $\gamma N \to MB$ interaction $v_{\gamma N,MB}$ and the $N^* \to MB$ verticies of Eq.(8) have been determined. In addition, most of the the electromagnetic form factors associated with $v_{\gamma N,MB}$ can be taken from previous works. Thus the $\gamma N \to N^*$ form factors will be the main unknown which will be determined by fitting the meson electro-production data.

Our first task is to find reasonable starting parameterization of the bare $\gamma N \to N^*$ form factors of Eq.(8). Instead of using the still not well-developed theoretical calculations of N^* form factors, we will proceed phenomenologically. First we note that with the strong verticies fixed by the fit to πN data, we can use Eq.(8) to calculate the meson cloud effects on $\gamma N \to N^*$ by calculating

$$\begin{aligned} \delta^{meson}_{N^*}(Q^2) &= \bar{\Gamma}_{N^*\to\gamma N}(Q^2) - \Gamma_{N^*\to\gamma N}(Q^2) \\ &= \sum_{MB} \int k^2 dk \bar{\Gamma}_{N^*\to MB}(k, E_R) G_{MB}(k, E_R) v_{MB,\gamma N}(k, q) \,, \end{aligned} \tag{11}$$

where E_R is the resonance position. Assuming that the dressed form factor $\bar{\Gamma}_{N^*\to\gamma N}(Q^2)$ is similar to the empirical form factors recently extracted by the CLAS collaboration[36] we can find some parameterizations of the bare form factor, such as the form used[33] in the study of $\Delta(1232)$ resonance

$$\Gamma_{N^*\to\gamma N}(Q^2) = (a + be^{-cQ^2}) F(Q^2) \,, \tag{12}$$

where $F(Q^2)$ is the usual dipole form factor

$$F(Q^2) = \frac{1}{(1 + Q^2/\Lambda^2_{N^*})^2} \,. \tag{13}$$

The resulting parameters a, b, c, and Λ_{N^*} will be the initial parameters which will be adjusted along with the not well-determined form factors associated with the non-resonant interaction $v_{MB,\gamma N}$ in the χ^2-fit to the meson production data.

Because of the large amount of the data we need to fit, we are proceeding with two separated but closely related efforts.

5.5 Analyses of πN, ηN and $\pi\pi N$ production data

With the initial parameters of the electromagnetic form factors chosen by the procedures described above, we then use our full computation codes defined by Eqs.(4) -(10) to fit the data of photo- and electro-production of π, η and $\pi\pi$. The resulting dressed form factor $\bar{\Gamma}_{N*\to\gamma N}(Q^2)$ can be compared with the values from the K-matrix model analysis of CLAS collaboration. The determined bare form factor $\Gamma_{N*\to\gamma N}(Q^2)$ can be compared with the predictions from hadron structure calculations which *do not* include the coupling with meson-baryon *scattering* states.

In this process, the K-matrix model fits by the CLAS collaboration will provide information in locating the ranges of our initial parameters, as explained above. Thus it is important that their analyses can include as much as coupled-channel effects which can be generated from our Eq.(5). A collaboration has been started between EBAC team and I. Aznauryan, V. Mokeev of CLAS collaboration to make progress in this direction. A project has been started to extend the combined analysis of 1π and 2π CLAS collaboration data to include explicit coupled-channel effects generated from a meson-exchange calculation at EBAC. This is aimed at improving the phenomenological aspects of the combined analyses of the CLAS collaboration and imposing more theoretical constraints in extracting the N^* parameters from the JLAB data. The results from the improved combined analyses will provide information for identifying the ranges of the bare N^* parameters, associated with the quark core wave function $\psi(q_c q_c q_c)$. We expect to perform this improved K-matrix model analysis by the end of 2006.

A good fit to the $\pi\pi N$ production data is crucial in this dynamical coupled-channel analysis mainly because $\pi\pi N$ is the dominant channel in the N^* region and can have large effects on all other production cross sections. This part of the computation program is most complex because it needs accurate calculations of the logarithmically divergent one-particle-exchange term $Z^{(E)}_{MB,M'B'}$ which has very large effects on two-pion production cross sections, as illustrated in Fig.15. At the present time, we are continuing the effort of Ref.[31] to perform detailed checks of this crucial part of the computation program. The fits to π, η, and $\pi\pi$ production data are expected to begin in the spring of 2007.

The results from the improved combined analyses will provide information for identifying the ranges of the bare N^* parameters, associated with the quark core wave function $\psi(q_c q_c q_c)$, in performing the dynamical coupled-channel analyses of all of the meson production data from CLAS by 2009. Therefore, by 2009 we will have coupled channel approach ready for combined analysis of the data on 1π and 2π electro-production from proposed experiments. Analysis of these two major exclusive channels in N^* excitation region will create most

reliable data on Q^2-evolution of resonance electro-couplings.

Capability of coupled channel approach to access bare N^* parameters will allow us to study in details transition from meson cloud to quark core as relevant degrees of freedom in N^* structure. We will examine the extent to which the $\gamma N \to N^*$ transition form factors extracted by the CLAS collaboration are consistent with the wave function composed by a quark core and meson cloud, and how high Q^2 the quark core wave function $\psi(q_c q_c q_c)$ can be described by the constituent quark models. In the first calculation for $\gamma N \to N^*(S_{11})$ at the photon point, significant meson cloud effects have been identified, as illustrated in Fig.16 from Ref.[35]. Complete coupled-channel calculations[37] for examining the meson cloud effects on the $\gamma N \to N^*$ form factors extracted by the CLAS collaboration will soon be completed.

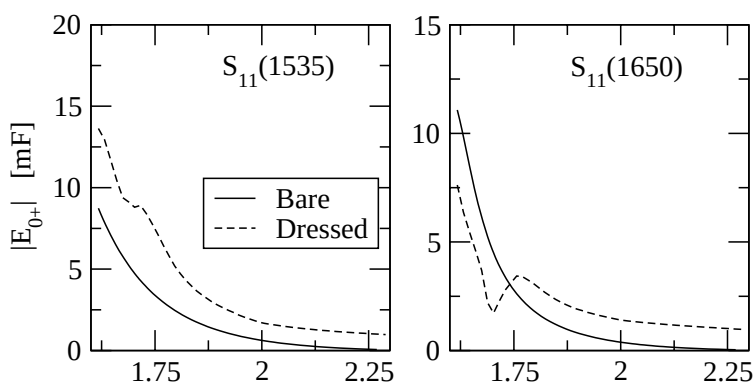

Figure 16: Meson cloud effect on $\gamma N \to N^*(S_{11})$ transition at Q^2=0. The results from [38]

Undoubtedly, the analyses of the data from the experiments proposed above will be complex and non-trivial. With the joint effort being made by EBAC and CLAS collaboration, the necessary coupled-channel analyses of the forthcoming data will be ready by the time 12 GeV upgrade is completed.

6 Single-Meson Electro-Production Experiment

6.1 Cross Section Measurement and Beam Time Estimates

We propose to extend the measurements of experiment E99-107 to $11\,GeV$ electron beam energy. In the conventional resonance region ($W \leq 2\,GeV$) the covered Q^2 range will extend beyond $12\,GeV^2$ (see Fig. 17). The differential cross section will be measured with a polarized electron beam as a function of the invariant mass W, the azimuthal hadronic angle ϕ_π, and the polar hadronic angle θ_π of the pion nucleon final-state [2]. In the one-photon-exchange approximation the fivefold differential cross section factorizes into the hadronic and the leptonic part [3]

$$\frac{d^5\sigma_v}{dk^\diamond_{20} d\Omega^\diamond_e d\Omega_\pi} = \Gamma_v \cdot \frac{d^2\sigma_v}{d\Omega_\pi}. \tag{14}$$

The virtual photon flux can be written as

$$\Gamma_v = \frac{\alpha}{2\pi^2} \frac{k^\diamond_{20}}{k^\diamond_{10}} \frac{k^\diamond_\gamma}{Q^2} \frac{1}{1-\varepsilon} \tag{15}$$

with the four momentum transfer $K^\mu = K^\mu_1 - K^\mu_2$, the corresponding squared four momentum transfer $-K_\mu K^\mu = Q^2$, and the incoming $K^\mu_1 = \{k_{10}, \vec{k}_1\}$ and outgoing $K^\mu_2 = \{k_{20}, \vec{k}_2\}$ electron four momenta, the equivalent photon energy

$$k^\diamond_\gamma = \frac{s - m^2}{2m} = \frac{W^2 - m^2}{2m} \tag{16}$$

and finally the degree of transverse polarization

$$\varepsilon = \left(1 + 2\,\frac{|\vec{k}^\diamond|^2}{Q^2}\,\tan^2\frac{\theta^\diamond_e}{2}\right)^{-1}. \tag{17}$$

In out-of-plane measurements the specific ϕ_π-dependences of the twofold hadronic cross section

$$\begin{aligned} \frac{d^2\sigma_v}{d\Omega_\pi} &= \sigma_T + \epsilon\sigma_L + \epsilon\sigma_{TT}\cos 2\phi_\pi + \sqrt{\epsilon(\epsilon+1)/2}\,\sigma_{TL}\cos\phi_\pi + \\ &\quad P_e\sqrt{\epsilon(1-\epsilon)/2}\,\sigma_{TL'}\sin\theta_\pi\sin\phi_\pi \end{aligned} \tag{18}$$

can be utilized to separate the four response functions, $\sigma_T + \epsilon\sigma_L$, σ_{TT}, σ_{TL}, and $\sigma_{TL'}$. A separation of σ_T and σ_L is not required for this proposal as the resonance couplings are known to be mostly transverse, thus the longitudinal amplitudes can be extracted with greater sensitivity from the interference terms σ_{TL} and $\sigma_{TL'}$ than from the total cross section. The specific θ_π-dependences of these four response functions on the other hand determine in the covered kinematic region the W and Q^2 evolution of the Legendre moments, which are the basis of the single-pion multipole or helicity amplitude analysis as described in chapter 6.2

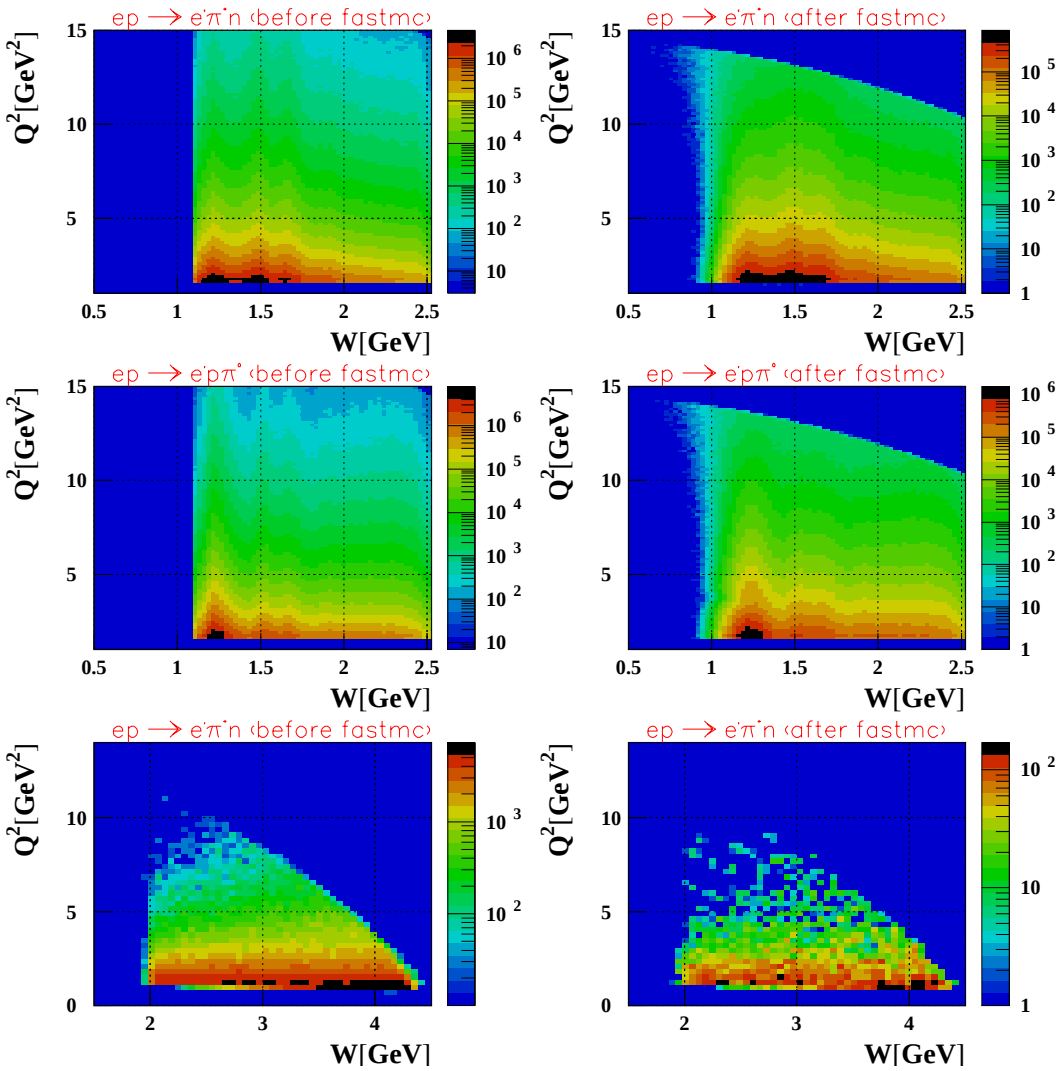

Figure 17: Kinematic coverage of CLAS12 in the resonance region for the exclusive one pion electro-production at $11\,GeV$ electron beam energy when e' and π^+ (upper and lower right panels) or e' and p (middle right panel) are detected in the CLAS12 fastmc simulation based on the Genova-EG (in the resonance region) or DIS (beyond the resonance region) event generator, and the corresponding Genova-EG (upper and middle left panels) and DIS (lower left panel) event generator data itself.

The beam time estimate for the $\gamma^* p \to \pi^+(n)(\pi^0 p, \eta p)$ reaction channel is not only based on the Genova-EG event generator [164] and the CLAS12 fastmc detector simulation, but also

[2]The described cross section decomposition applies more generally to any single-meson nucleon final-state.

[3]Variables in the lab frame (LAB) are marked with diamonds $^\diamond$ and all unmarked variables are in the center-of-mass frame (CM).

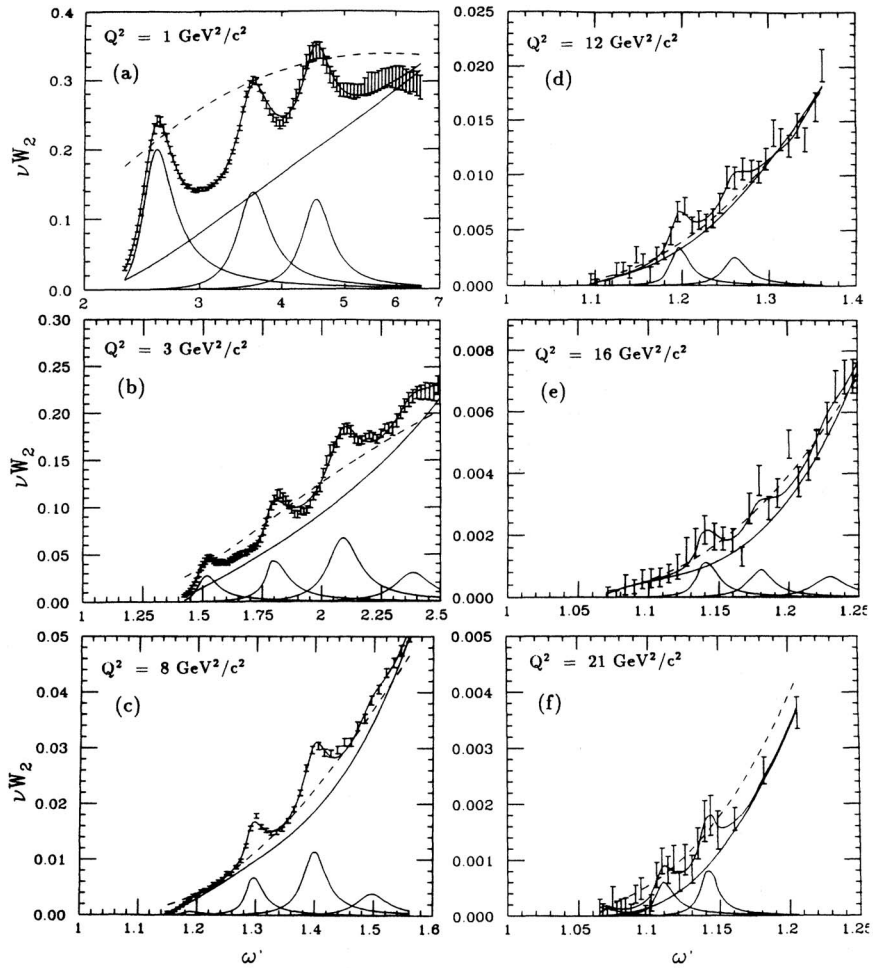

Figure 18: The structure function νW_2 versus ω' inclusive inelastic scattering in the resonance region for various values of nominal Q^2, where $\omega' \equiv 1 + W^2/Q^2$ [60, 65, 66, 100, 104]. The solid curves are fits to the data that include only $\Delta(1232)$, $S_{11}(1535)$, and $F_{15}(1680)$ resonance contributions [108]. The dashed curves are fits to the data in the scaling region extrapolated down to the resonance region.

on the measured exclusive [97] and inclusive [108] cross sections. An overview of the inclusive inelastic scattering in the resonance region, as in Fig. 18, demonstrates that at all Q^2 even up to $21\,GeV^2$ resonance structures are visible and that the νW_2 structure function result at $Q^2 = 3\,GeV^2$ agrees with the recent total inclusive cross section at $Q^2 = 2.915\,GeV^2$ [97]. In addition the peak strength in the second resonance region attributed to the $S_{11}(1535)$ and in the third resonance region attributed to the $F_{15}(1680)$ scale like the dipole form factor given by $G_{dip} = \mu_p(1 + Q^2/0.71)^{-2}$ [108]. This experimental result justifies the use of the Genova-

EG event generator beyond the first resonance region, since it also assumes dipole behavior for the Q^2 evolution of the transition form factors. The appropriate [4] normalization of the simulated and acceptance corrected total number of events for $11\,GeV$ electron beam energy to the measured one for $5.75\,GeV$, both at $Q^2 = 3\,GeV^2$, accomplishes a more precise beam time estimate that is independent of the cross section as it is assumed by the Genova-EG event generator.

(k_{10}, Q^2)	$(5.75\,GeV, 3.0 \pm 0.5\,GeV^2)$	$(11\,GeV, 3.0 \pm 0.5\,GeV^2)$	$(11\,GeV, 12.0 \pm 0.5\,GeV^2)$
$N_{ac}^{\pi^+}$	$1.12 \cdot 10^6$	$1.72 \cdot 10^7$	$6.98 \cdot 10^4$
N^{π^+}	$1.41 \cdot 10^5$	$6.26 \cdot 10^6$	$5.18 \cdot 10^4$
$N^{\pi^0 p}$	-	$4.65 \cdot 10^5$	$1.45 \cdot 10^4$
$N^{\eta p}$	-	$1.72 \cdot 10^4$	$1.77 \cdot 10^4$

Table 1: Total number of events N for the $\pi^+(n)$, $\pi^0 p$, and ηp final state and the acceptance corrected one $N_{ac}^{\pi^+}$ for specific kinematic bins focusing on the $S_{11}(1535)$ resonance, with $W = 1535 \pm 100\,MeV$, as an example for the anticipated statistics at an electron beam energy of $k_{10} = 11\,GeV$ gathered in $60\,d$ compared to the measured ones at $k_{10} = 5.75\,GeV$.

Table 1 summarizes the anticipated number of measured events for a specific W and Q^2 bin centered at the $S_{11}(1535)$ resonance. A more general overview is presented in Fig. 17. It shows the generated versus accepted W and Q^2 coverage for both the Genova-EG (middle panels) and the DIS [5] (lower panels) event generator, where the ratio of the accepted over generated events gives the θ and ϕ integrated acceptance. But for any specific W and Q^2 bin we can also generate the corresponding θ and ϕ dependent acceptance functions. Figs. 19-24 present for each final state channel a set of exemplifying plots of the W, Q^2, ϕ, and θ evolutions of the CLAS12 acceptance.

The acceptance and consequently the total number of events, as presented in Table 1, are for the $\pi^0 p$ and ηp final state significantly smaller than for the $\pi^+(n)$ reaction channel. This is due to the fact, that for the neutral meson production channels the single-photon background can only be separated, when both the proton and the neutral meson are detected, which reduces the combined acceptance especially at low momentum transfers, see Figs. 21-24. The missing mass resolution for the neutron in the $\pi^+(n)$ final state is typically better than $40\,MeV$ and increases only for large momentum transfers to a maximum of $80\,MeV$ at $Q^2 = 12\,GeV^2$. The corresponding plots and the neutron missing mass itself are shown in Fig. 25.

[4] Taking the different virtual photon fluxes and electron scattering solid angles for both electron beam energies $5.75\,GeV$ and $11\,GeV$ into account.

[5] Deep inelastic scattering.

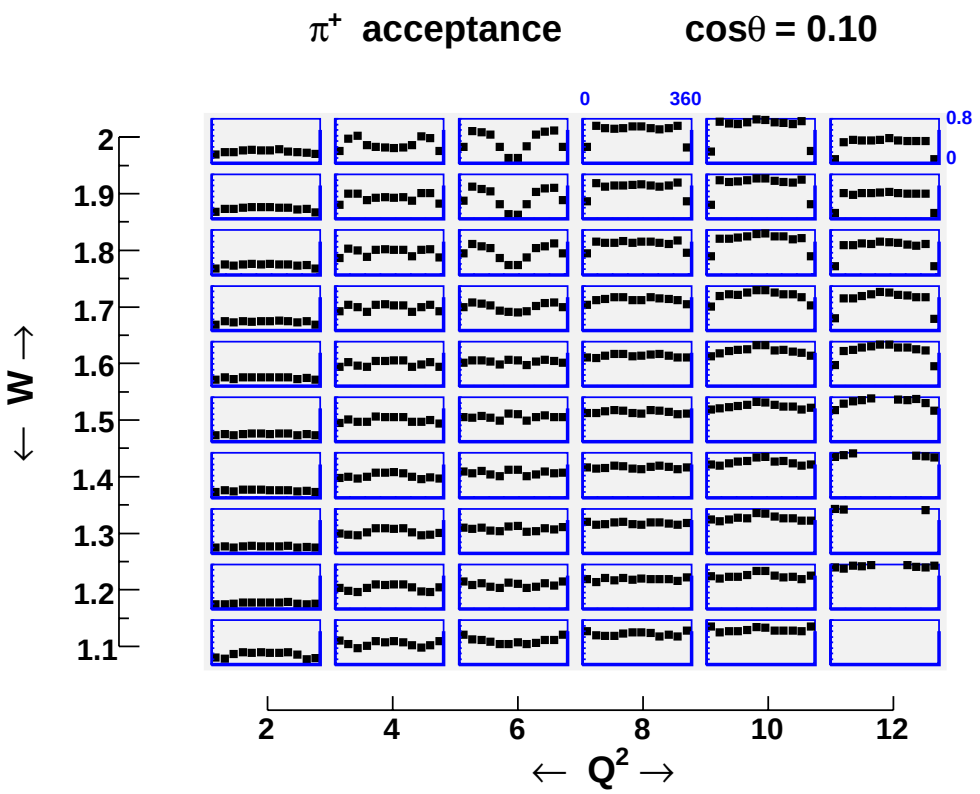

Figure 19: ϕ_π evolution of the π^+ acceptance in the forward $cos\theta_\pi = 0.1 \pm 0.1$ bin for the resonance region and the proposed Q^2 range.

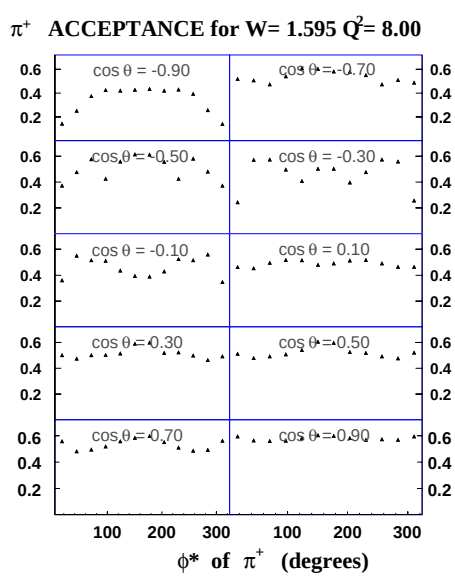

Figure 20: ϕ_π evolution of the π^+ acceptance in a specific W and Q^2 bin for the full $cos\theta_\pi$ range.

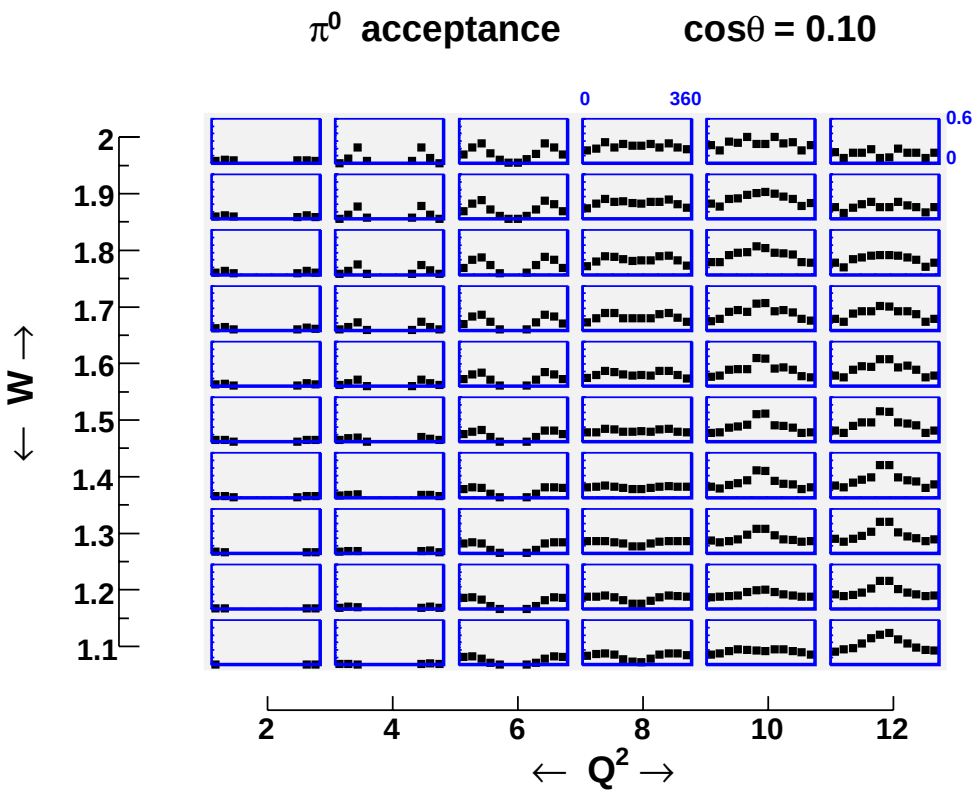

Figure 21: ϕ_π evolution of the π^0 acceptance in the forward $cos\theta_\pi = 0.1 \pm 0.1$ bin for the resonance region and the proposed Q^2 range.

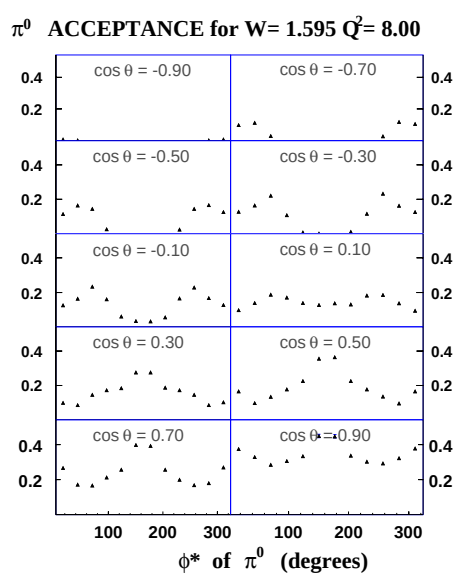

Figure 22: ϕ_π evolution of the π^0 acceptance in a specific W and Q^2 bin for the full $cos\theta_\pi$ range.

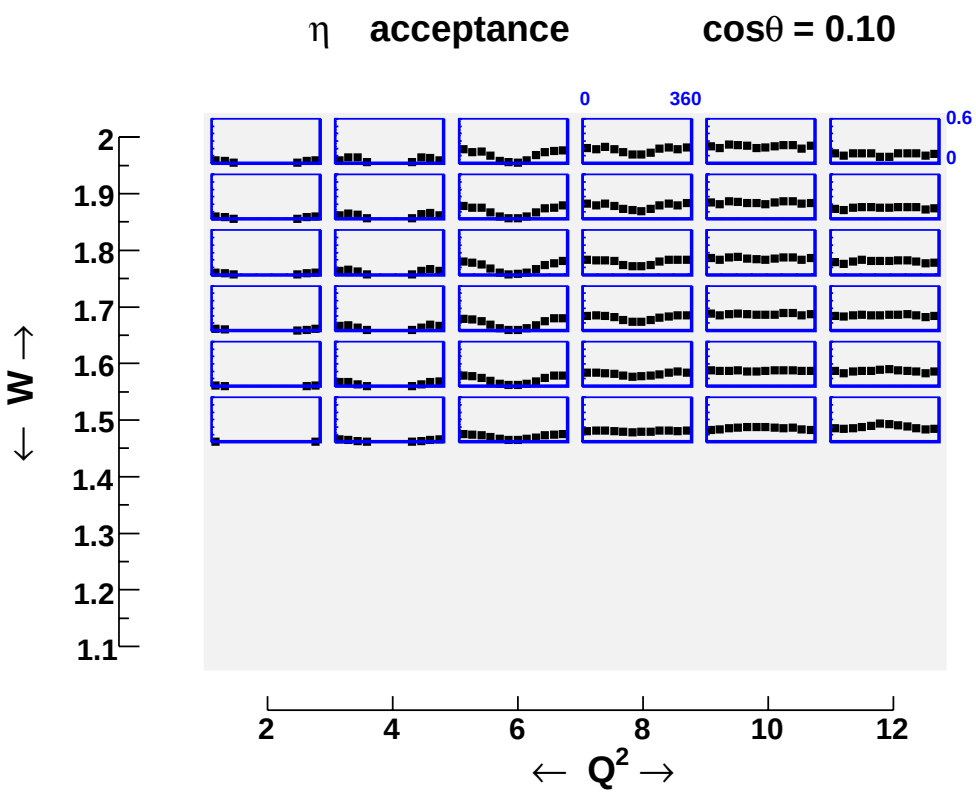

Figure 23: ϕ_η evolution of the η acceptance in the forward $cos\theta_\eta = 0.1 \pm 0.1$ bin for the resonance region and the proposed Q^2 range.

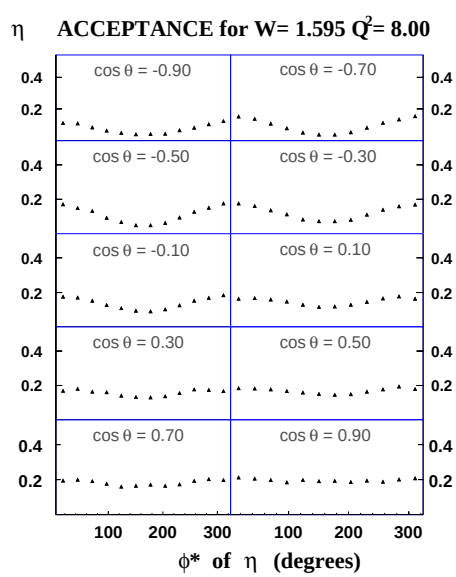

Figure 24: ϕ_η evolution of the η acceptance in a specific W and Q^2 bin for the full $cos\theta_\eta$ range.

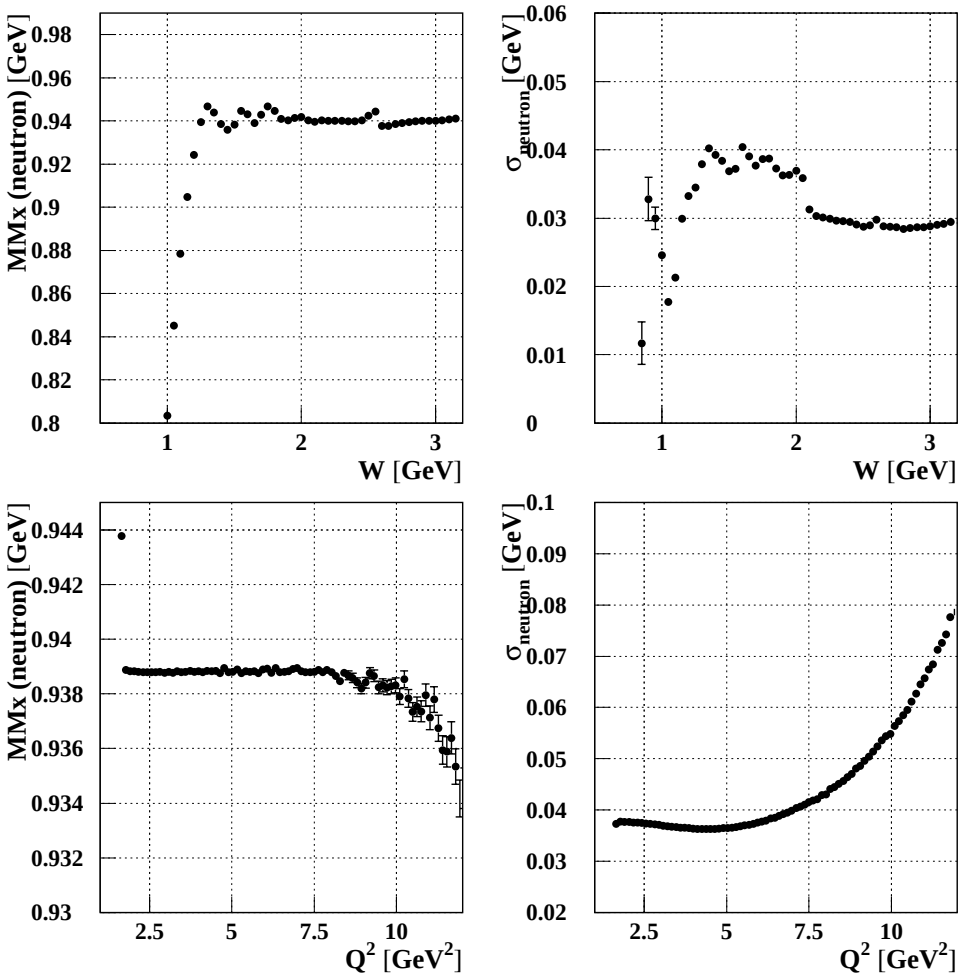

Figure 25: Missing mass (right panels) and missing mass resolution (left panels) for the $\gamma^* p \to \pi^+(n)$ reaction based on the Genova-EG event generator and the CLAS12 fastmc simulation in dependence of the invariant mass W (upper panels) and the momentum transfer Q^2 (lower panels).

6.2 Data Analysis

Over the past 40 years, our knowledge of electromagnetic excitations of nucleon resonances was, with the exception of the $S_{11}(1535)$, dominantly based on the single-pion photo- and electro-production [70, 99]. This reaction has been the subject of extensive theoretical studies, and a series of models and approaches were developed for its investigation from threshold to $W = 2\,GeV$. The Unitary Isobar Model in 1999 [76], also known as MAID, is widely used for description of single-pion electro-production data since the very beginning in 1999. Later this model has been modified [51] by the incorporation of Regge poles, which enables a good

description of all photo-production multipole amplitudes with $l \leq 3$ up to $W = 2\,GeV$ using a unified Breit-Wigner parametrization of the resonance contributions in the form as proposed by Walker [111]. The Unitary Isobar Model (UIM) [51] has been successfully used for the analysis [36, 52, 53] of the CLAS [77, 84–86, 97] and the world data on the cross sections and longitudinally polarized electron beam asymmetries for the reactions $p(\vec{e}, e'p)\pi^0$ and $p(\vec{e}, e'n)\pi^+$ in the first, second, and third resonance region. The quality of the obtained descriptions are characterized by the following χ^2 values: $\chi^2 < 1.6$ at $Q^2 = 0.4$ and $0.65\,GeV^2$ and $\chi^2 < 2.5$ at $1.72 < Q^2 < 4.16\,GeV^2$. In the analyses [36, 52, 53], the Q^2 evolution of all resonances with $M < 1.75\,GeV$ has been established up to a Q^2 of $4.5\,GeV^2$.

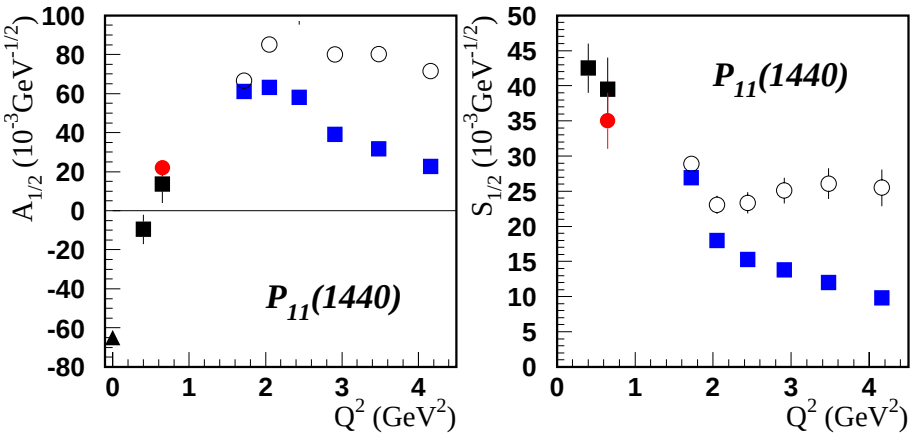

Figure 26: Helicity amplitudes for the $P_{11}(1440)$ electro-excitation on the proton found in our analyses [36, 52, 53]: filled black squares are from analysis [36] of CLAS data [77, 84–86], filled red circles are obtained from the combined analysis [52] of the CLAS π and 2π electro-production data, filled blue squares are obtained in the analysis [53] of CLAS π^+ electro-production data [97], and the filled black triangle at $Q^2 = 0$ is the RPP estimate [99]. The open black circles are the results at $Q^2 \geq 1.72\,GeV^2$ multiplied by $Q^2/1.6$ to linearize the Q^2 dependence of the helicity amplitudes at large Q^2.

Figure 26 shows the results for $P_{11}(1440)$resonances in the second and third resonance region obtained in our analyses [36, 52, 53]. In order to extrapolate the results to higher Q^2, we tried to linearize the shape of the Q^2 evolution of the $\gamma p \to N^*$ helicity amplitudes at $Q^2 \geq 1.72\,GeV^2$. The open circles in Figs. 26 represent the helicity amplitudes multiplied by $(Q^2/1.6)^a$. It turns out that this product of the helicity amplitudes with $(Q^2/1.6)^a$ reveals approximately constant behavior, if $a \simeq 1$ (1.5) is chosen in case of the $\frac{1}{2}$ ($\frac{3}{2}$) amplitudes. A similar behavior is also revealed by the $\frac{1}{2}$ transverse amplitudes of the resonances $P_{33}(1600)$, $S_{31}(1620)$, $S_{11}(1650)$, $D_{13}(1700)$, $D_{33}(1700)$, and $P_{13}(1720)$.

The background of the Unitary Isobar Models [51, 76] consists of the Born term, nucleon exchanges in the s- and u-channels and π exchange in the t-channel, as well as ρ and ω exchanges. The Born term contributions are constricted by the proton and neutron magnetic and electric form factors, as well as the pion form factor. The estimations of the background

contributions at higher Q^2, is based on the experimental results and is carried out according to the following six steps.

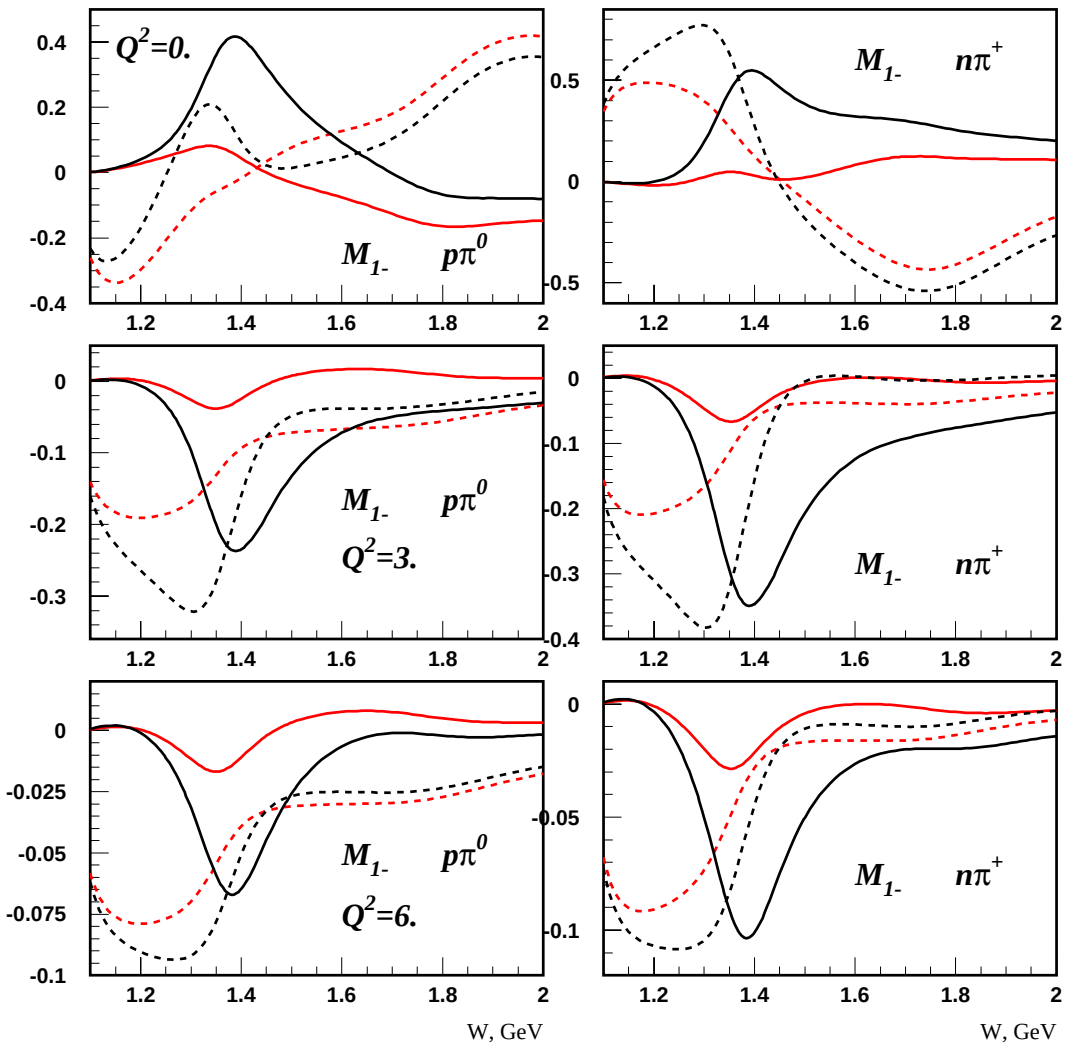

Figure 27: The M_{1-} multipole amplitude for the reactions $\gamma^* p \to p\pi^0$ (left) and $n\pi^+$ (right) at $Q^2 = 0,\ 3$, and $6\,GeV^2$. Black curves are the total amplitudes, red curves represent the background, and solid (dashed) curves are the imaginary (real) parts of the amplitudes.

1) Measurements of the proton magnetic form factor $G_{M_p}(Q^2)$ have been carried out over the last 50 years [47, 54, 55, 91, 101, 107, 113]. They show up to a Q^2 of $10\,GeV^2$, that $G_{M_p}(Q^2)$ follows the dipole form

$$\frac{G_{M_p}(Q^2)}{\mu_p} = G_d(Q^2) = \frac{1}{(1+\frac{Q^2}{0.71GeV^2})^2}. \tag{19}$$

There are slight deviations from this behavior of $3\% - 4\%$, which are reproduced by the parametrization [61] of existing the data.

2) The ratio of the electric and magnetic proton form factors has been recently measured at Jefferson Lab up to $Q^2 = 5.6\,GeV^2$ [41, 79]. These measurements show that a straight line fit can be applied to the ratio $\mu_p \frac{G_{E_p}(Q^2)}{G_{M_p}(Q^2)}$ in the range of $0.5\,GeV^2 < Q^2 < 5.6\,GeV^2$.

$$\mu_p \frac{G_{E_p}(Q^2)}{G_{M_p}(Q^2)} = 1 - 0.13(Q^2 - 0.04) \tag{20}$$

The experimental error of this ratio increases 11%, 14%, 31% with increasing $Q^2 = 3.97,\ 4.75,\ 5.54\,GeV^2$, respectively.

3) The neutron magnetic form factor $G_{M_n}(Q^2)$ is measured up to $Q^2 = 10\,GeV^2$ [93, 103]. In this Q^2 range, the ratio $\frac{G_{M_n}(Q^2)}{\mu_n}$ is close to the dipole form with the tendency to fall faster than $G_d(Q^2)$ starting at $Q^2 = 3\,GeV^2$

$$\begin{aligned} \frac{G_{M_n}(Q^2)}{\mu_n G_d(Q^2)} &\hat{=} 0.967 \pm 0.031 \pm 0.052,\ Q^2 = 3.25\,GeV^2\ [93], \\ &\hat{=} 0.923 \pm 0.048 \pm 0.065,\ Q^2 = 4\,GeV^2\ [93], \\ &\hat{=} 0.91 \pm 0.05,\ Q^2 = 6\,GeV^2\ [103], \\ &\hat{=} 0.71 \pm 0.12,\ Q^2 = 8\,GeV^2\ [103]. \end{aligned} \tag{21}$$

4) The neutron electric form factor $G_{E_n}(Q^2)$ is measured up to $Q^2 = 1.5\,GeV^2$ and reviewed in [75]. Taking into account the results of these measurements and the falloff of $G_{E_n}(Q^2)$ predicted by theoretical models [75], we have parametrized this form factor in two ways:

$$G_{E_n}(Q^2) = \frac{0.06}{Q^2/0.5} \quad \text{or} \quad \frac{0.06}{\sqrt{Q^2/0.5}} \quad \text{for} \quad Q^2 > 0.5\ GeV^2. \tag{22}$$

5) The pion form factor $G_\pi(Q^2)$ has been studied for Q^2 values from 0.4 to $9.8\,GeV^2$ at CEA/Cornell [56, 57] and more recently at JLab at $Q^2 = 0.6 - 1.6\,GeV^2$ [40]. All these measurements show that the Q^2 dependence of $G_\pi(Q^2)$ can be described by the simple monopole form

$$\begin{aligned} G_\pi(Q^2) &\cong G_m(Q^2), \\ G_m(Q^2) &= \frac{1}{1 + Q^2/0.46}\ [56, 57], \\ G_m(Q^2) &= \frac{1}{1 + Q^2/0.54}\ [40]. \end{aligned} \tag{23}$$

6) There are no measurements of the form factors $G_{\rho(\omega)\to\pi\gamma}(Q^2)$, which determine t-channel ρ and ω exchanges. However, investigations made using both QCD sum rules [78] and quark models [49] predict that the Q^2 dependence of these form factors follows closely the dipole form. Therefore our corresponding background estimations proceeds from the assumption that

$$G_{\rho(\omega)\to\pi\gamma}(Q^2) \cong G_d(Q^2). \tag{24}$$

Figure. 27 shows the M_{1-} multipole amplitudes for the reactions $\gamma^* p \to p\pi^0$ and $n\pi^+$ at $Q^2 = 0,\ 3,$ and $6\,GeV^2$. The results at $Q^2 = 0$ and $3\,GeV^2$ correspond to our analyses [51, 53]. The results at $Q^2 = 6\,GeV^2$ are based on our extrapolations of the resonance contributions as found at $Q^2 = 1.72 - 4.16\,GeV^2$ in the analysis [53] of CLAS $\gamma^* p \to n\pi^+$ data [97]. The background at $Q^2 = 6\,GeV^2$ is built using the information on the form factors as listed above. All the uncertainties in the form factors have been taken into account, including a 50% uncertainty for $G_{\rho(\omega)\to\pi\gamma}(Q^2)$ in 6). All these uncertainties practically do not affect M_{1-} multipole amplitude and have very small influence on the background of E_{0+}.

From the results presented in Fig. 27 we can draw the interesting and encouraging conclusion that with increasing Q^2 the resonance signals become much stronger in comparison to the background. Such behavior of the relative resonances-to-background contributions is connected to the fact that the Q^2 dependence of the background is mainly determined by the proton form factors, which fall as (or stronger than) the dipole form factor, whereas most of resonance amplitudes in the second and third resonance region seem to fall as $1/Q^2$. So that the proposed Q^2 region presents a unique and new opportunity to distinguish resonance from background contributions and to investigate the Q^2 evolution of the N^* electro-excitation amplitudes.

7 Double Charged Pion Data Analysis and Beam Time Estimates

7.1 Double charged pion exclusive channel

7.1.1 Experimental studies of 2π photo- electro-production in N^* excitation region

Data on 2π production by real and virtual photons already provided considerable amount of information for the evaluation of N^* electro-couplings at photon virtualities Q^2 below 1.5 GeV^2. Available data consist of old bubble chamber measurements [143] at the photon point and recent real photon data collected at Bonn, GRAAL, MAMI [120–123, 125–128]. Most detailed 2π electro-production data were obtained with the CLAS detector [115, 119] These data cover the kinematics range in W from 1.3 GeV to 1.9 GeV and for photon virtualities Q^2 from 0.2 GeV^2 to 1.5 GeV^2. Fully integrated 2π electro-production cross section data measured with CLAS are shown on Fig. 29.

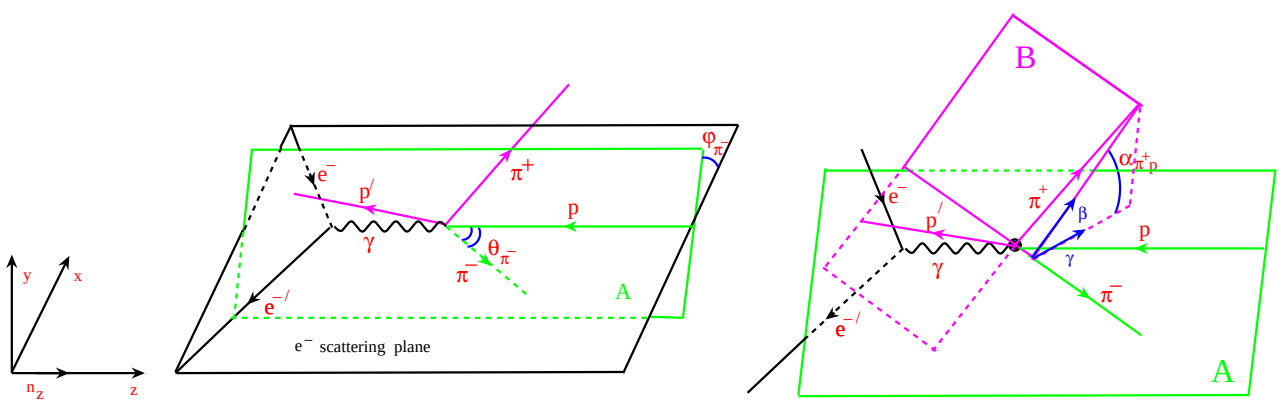

Figure 28: Angular variables used in analysis of the CLAS data on 2π production.

The description of the $\pi^-\pi^+p$ final states requires five kinematic variables, which may be chosen to be two invariant masses of the final hadrons, the solid angle describing the momentum of one of the hadrons, and the angle between two planes. The three-momenta of two pairs of the final hadrons are chosen to define these two planes. The choice of the five variables is not unique. The angular variables used in the CLAS analysis are shown on Fig. 28. In each $(W\&Q^2)$ bin covered the following single differential cross-sections integrated over 4 other variables were obtained:

- $\pi^-\pi^+$, π^+p, π^-p mass distributions
- π^+, π^-, p CM-angular distributions
- 3 distributions over angles between two planes, composed by two pairs of 3-momenta of the final hadron for 3 various choices of hadron pairs: $\frac{d\sigma}{d\alpha}$. The angle α is shown on Fig. 28..

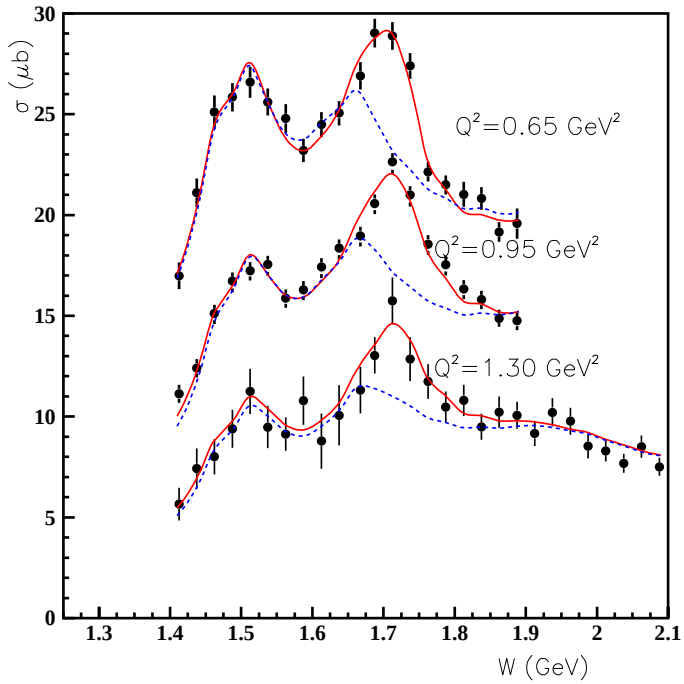

Figure 29: Total double charged pion virtual photon cross-sections. Fit of CLAS data [115] within the framework of JM05 model [142] is shown by solid lines. Dashed lines correspond to JM05 calculation with $3/2^+(1720)$ candidate state taken out.

A detailed set of measurements of unpolarized observables is available for the first time from the CLAS detector, with acceptance close to 4π. A similar set of measurements can be expected with CLAS12. It is a considerable advantage for analyzing the $\pi^+\pi^-p$ final state to have 9 single differential cross-sections in each $W\&Q^2$ bin. The large variety of unpolarized observables from the 2π data makes it possible to establish the main contributing mechanisms from a combined fit to cross sections and to isolate the resonant part. A phenomenological approach, referred below as JM05 model, was developed in collaboration between Hall B at Jefferson Lab and the Nuclear Physics Institute at Moscow Sate University [142, 144–148], which allowed us to access N^* parameters from a global fit to all available 2π observables.

7.1.2 Physics analysis of double pion exclusive photo- and electro-production

Analysis of the 2π exclusive channel with the goal of extracting the N^* parameters represents a challenging task. The signals from nucleon resonances are embedded in considerable non-resonant mechanisms, which have even dominant contributions at low Q^2. Attempts to analyze 2π photo- and electro-production, using model independent partial wave decomposition [116, 149] face considerable difficulties. Analysis of preliminary CLAS 2π photo-production

data within the framework of partial wave decomposition [116] showed, that even using a very restricted angular momentum basis with total angular momentum up to 5/2, we need to involve several tens of partial waves to get a reasonable data description at W<2.0 GeV. The search for new states requires extension of the W-coverage up to 3.0 GeV making the pure partial wave approach an even more challenging task. The more limited statistic makes the partial wave analysis difficult to apply to electro-production 2π data, especially at high Q^2. Moreover, even if a successful separation among all partial waves would be achieved, we still need to isolate resonant and non-resonant mechanisms in each partial wave to access N^* electromagnetic and/or hadronic parameters. There is no model independent way to disentangle comparable resonant/non-resonant contributions. This is the most common situation for 2π photo- and electro-production amplitudes at W>1.6 GeV. Therefore, reaction models have to be used in the analysis of 2π electro-production data, particularly at high W and Q^2

Several model approaches [151–158] were developed for the description of 2π photo- and electro-production following the pioneering paper of Luke and Soding [150]. These approaches used tree level meson-baryon diagrams with various parametrization of electromagnetic/hadronic vertex functions, and meson and baryon propagators. Most of them were developed for N^* studies in the mass range below 1.6 GeV. The contributions from excited states of higher masses were limited to just a few particular states. None of these approaches includes contributions from all well established proton excitations with observed two pion hadronic decays. Most detailed and sophisticated treatment of the non-resonant mechanisms in 2π photo- and electro-production at W<1.6 GeV was achieved in the work of the Valencia group [155–157]. This approach was successfully employed in the description of a limited set of world data [123, 125–128] available before the CLAS measurements at low W. Another approach [152] was successfully used in the description of GRAAL data on $2\pi^0$ photo-production [122]. However, none of these approaches were applied in the analysis of entire set of hadronic unpolarized observables for the 2πp final state, described in the Section 7.1.1. Therefore, the capability of these models to describe entire sets of the single differential cross-sections in 2π electro-production is an open question. On the other hand, the successful description of all single differential cross-sections combined is critical for a credible isolation of the resonant parts in double pion production amplitudes. Moreover, as W increases more mechanisms may contribute to 2π production. Also the interaction with open inelastic channels in the initial and final states (ISI&FSI) become more important. It is difficult to see that approaches, based on analysis of a limited set of observables at low W, with absent [155–157] or oversimplified ISI&FSI treatment [150, 152] would allow a credible separation of resonant and non-resonant mechanisms at W>1.6 GeV, which is needed for the studies of high lying nucleon excitations.

To facilitate phenomenological studies of nucleon resonances in the entire N^* excitation region, especially at masses above 1.6 GeV, the JM05 model was developed [142].

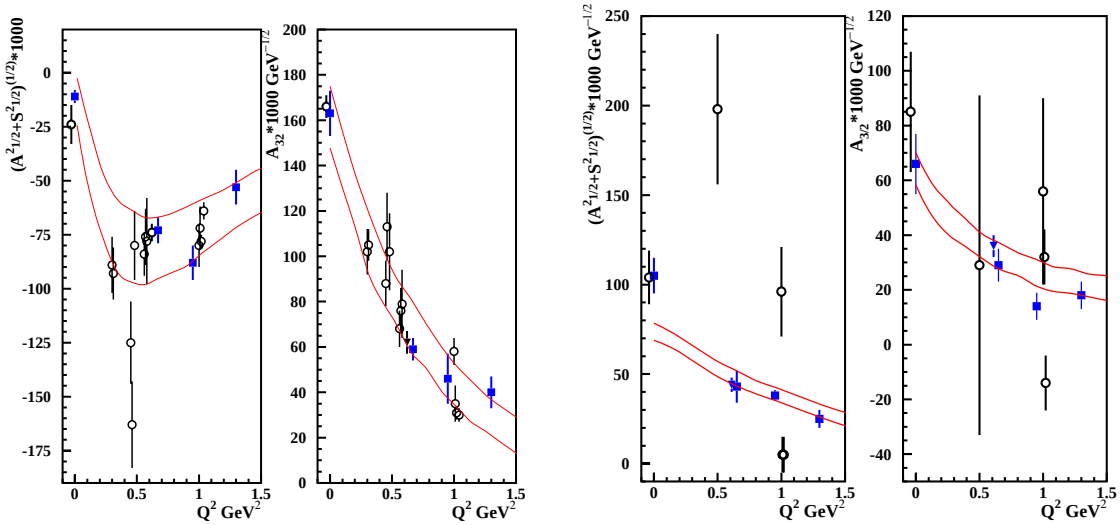

Figure 30: Photo- and electro-couplings for D13(1500) and D33(1700): extracted from CLAS 2π data within the framework of JM05 [142] are shown by filled squares with error bars, while world data from 1π exclusive channel are shown by open circles with error bars. Area restricted by lines represents values of N^* electromagnetic form factors, obtained in the fit within the framework of the SQTM approach [132]

.

7.1.3 Essentials of JM05 model and 2π CLAS data analysis

We developed a phenomenological approach, capable to establish all relevant mechanisms contributing to the 2π photo- and electro-production from the combined analysis of all measured observables. We implemented particular meson-baryon mechanisms, based on their manifestation in observables as slopes in angular distributions or visible structures in invariant mass distributions. We described these mechanisms by the simplest amplitudes compatible with the data taking into account Lorentz invariance, P,C,T symmetries. Exchange processes that were observed in the data were described either by Reggetiezed propagators or by an exponential parametrization. We also used restrictions, imposed by gauge invariance for meson baryon diagrams in $\pi\Delta$ isobar channels.

The complexity of 2π production mechanisms was described by superposition of the following isobar channels:

$$\gamma p \to \pi^- \Delta^{++} \to \pi^- \pi^+ p, \tag{25}$$
$$\gamma p \to \pi^+ \Delta^0 \to \pi^+ \pi^- p, \tag{26}$$
$$\gamma p \to \rho^0 p \to \pi^+ \pi^- p, \tag{27}$$
$$\gamma p \to \pi^+ D^0_{13}(1520) \to \pi^+ \pi^- p, \tag{28}$$
$$\gamma p \to \pi^+ F^0_{15}(1685) \to \pi^+ \pi^- p, \tag{29}$$

N^*, Δ^*	M, GeV	Γ_{tot} GeV	$BF_{\pi\Delta}$ %	$BF_{\rho p}$ %
$P_{11}(1440)$	1.440	0.350	22.	0.
$D_{13}(1520)$	1.520	*var.*	*var.*	*var.*
$S_{31}(1620)$	1.620	0.150	62.	29.
$P_{33}(1600)$	*var*	*var.*	*var.*	*var.*
$S_{11}(1650)$	1.650	0.167	2.	3.
$D_{15}(1675)$	1.675	0.160	53.	0.
$F_{15}(1680)$	1.680	0.130	22.	7.
$D_{13}(1700)$	*var.*	*var.*	*var.*	*var.*
$D_{33}(1700)$	1.700	0.300	78.	8.
$P_{13}(1720)$	*var.*	*var.*	*var.*	*var.*
$3/2^+(1720) cand.$	*var.*	*var.*	*var.*	*var.*
$F_{35}(1905)$	*var.*	*var.*	*var.*	*var.*
$P_{33}(1920)$	*var.*	*var.*	*var.*	*var.*
$F_{37}(1950)$	*var.*	*var.*	*var.*	*var.*

Table 2: List of resonances included to JM05 and theirs hadronic properties: total decay widths Γ_{tot}, branching fractions (BF) to $\pi\Delta$ and ρp final states. The quoted values are taken from RPP [129]. The quantities labeled as "var." were fitted to the CLAS 2π data.

$$\gamma p \to \pi^- P_{33}^{++}(1600) \to \pi^- \pi^+ p. \tag{30}$$

Manifestation of all these isobar channels were clearly seen in observables [142, 144–148] Quasi-two-body processes in the channels (25),(26),(27) were described as superposition of N^* excitation in s-channel and non-resonant mechanisms.

The resonant parts in these channels (25),(26),(27) were evaluated using a Breit-Wigner ansatz, described in [144, 145]. We included all well established excited states of 4 star PDG status plus 3 star states listed in the Table 2

N^* hadronic decay amplitudes were estimated from the data on partial decay width available from the analysis of experiments with hadronic probes. However, for high lying nucleon excitations these hadronic data are too uncertain and we adjusted hadronic parameters for such states to the CLAS data (see Table 2). N^* electromagnetic form factors were treated as free parameters and fitted to the data.

Analysis of CLAS 2π electro-production data [115] revealed signals from a possible new $3/2^+(1720)$ state. Dashed lines on Fig. 29 represent best data fit without the contributions from this state. Assuming the contributions from conventional states only,a reasonable description of all observables was achieved [115] except in the area around 1.7 GeV. Implementation of a new baryon state candidate with electromagnetic and hadronic parameters derived from the data fit allowed us to reproduce the data reasonably well in the entire kinematics covered by the measurement. The $3/2^+(1720)$ candidate state was included in all further CLAS data analysis.

Non-resonant mechanisms of various isobar channels are described in [145],[147], [142], [161].

In addition to the isobar channels (25),(26),(27), (28),(29),(30) the JM05 model includes remaining direct 2π production mechanisms, when $\pi^-\pi^+p$ final state is produced without the formation of unstable intermediate particles. Phenomenological analysis of the entire set of single differential cross-section measured with CLAS [115, 119] allowed us to access the dynamics of the remaining mechanisms. Parametrization for their amplitudes is given in [142].

The JM05 model provided reasonable description of all available CLAS/world data on 2π photo- and electro-production at W< 1.9 GeV and at photon virtualities Q^2<1.5 GeV^2. $\chi^2 perd.p. < 3.0$ was achieved in the fit of all single differential cross-section, averaged over all W bins in each Q^2 interval separately. Since data uncertainties were estimated based on statistics errors only, such values of $\chi^2 perd.p.$ look quite reasonable. Total $\pi^-\pi^+p$ cross-sections calculated with the framework of JM05 model [142] in comparison with CLAS data [115, 119] is shown on Fig. 29.

Successful description of all CLAS/world data on unpolarized observables was achieved within the framework of JM05 without any need for additional processes of unknown dynamics. The contributions from additional processes on top of implemented to JM05 was consistent with zero in entire N^* excitation region covered by CLAS/world measurements. Therefore, for the first time we developed phenomenological approach for description of 2π electro-production in N^* excitation region with most complete accounting for all relevant non-resonant mechanisms.

Important feature of JM05 is capability to pin down contributing mechanisms from the data fit. We expect, that this approach being applied to the data at high Q^2 will allow us to establish new, still unknown mechanisms, contributed to the 2π electro-production at high photon virtualities $5<Q^2<10GeV^2$. Therefore, we are suggesting JM05 model as general framework for physics analysis of 2π electro-production data from CLAS12 with a goal to determine Q^2-evolution of N^* electro-couplings. Critical requirement for experiment is capability to obtain entire set of single differential cross-sections for $\pi^-\pi^+p$ final state.

Information on cross-sections and/or amplitudes of isobar channels (25),(26),(27), (28), (29),(30, which will be obtained within the framework JM05, is of particular interest for other parts of CLAS12 Program as target fragmentation studies [162].

7.1.4 N^* studies at intermediate photon virtuality within the framework of JM05 model

Combined analysis of 2π single differential cross-sections within the framework of JM05 allowed us to isolate resonant part of cross-sections. Manifestation of resonant and non-resonant mechanisms in single differential cross-sections are shown in Fig. 31. The curves represent best data fit with minimal χ^2. Both resonant and non-resonant mechanisms have very different manifestations in various observables, which are highly correlated by reaction dynamics. Moreover, resonant/non-resonant part behavior look very different in π^- angular

and $\pi^-\pi^+$, π^-p mass distributions and quite different in π^+p mass distributions. Combined fit of all these observables provided reliable isolation of resonance mechanisms. Dashed and solid lines in Fig. 31 correspond to two different ways for modeling of additional non-resonant contributions to $\pi\Delta$ isobar channels [163]. For both ways of non-resonant mechanisms modeling we achieved almost identical and reasonable data description with the same values of N^* electro-couplings. It proves reasonable parametrization of phenomenological terms in JM05 as well as credibility of resonant/non-resonant mechanism separation.

Moreover, N^* electro-couplings, determined in the CLAS 2π data fit, also provide reasonable description of all observables measured with CLAS in 1π electro-production at $Q^2 = 0.65GeV^2$ [52]. Since 1π and 2π exclusive channels are major contributors in N^* excitation region with completely different non-resonant mechanisms, it is most compelling evidence for reliable isolation of resonant contributions, achieved in JM05.

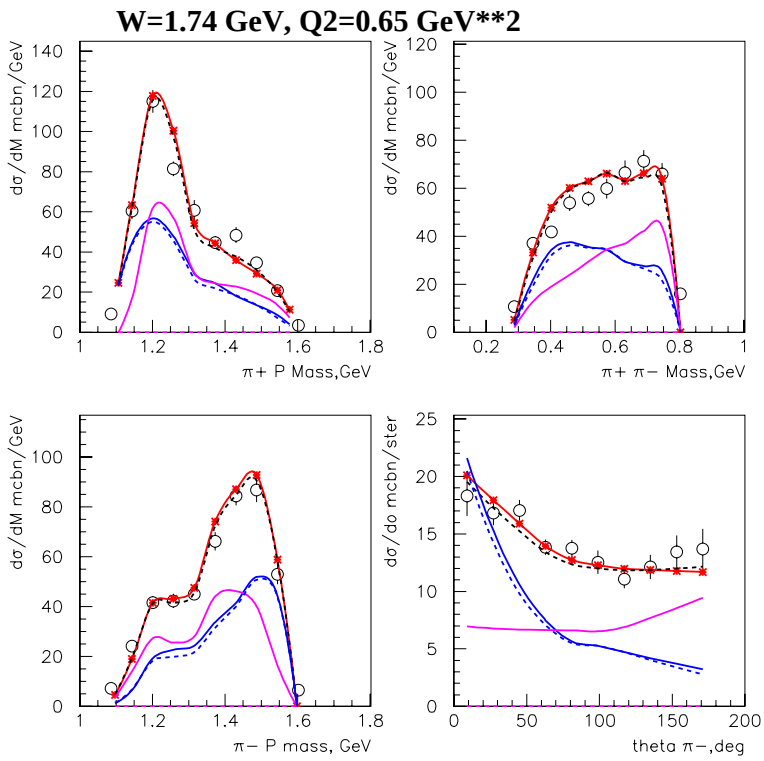

Figure 31: Separation between resonant and non-resonant parts of cross-sections. Resonant and non-resonant contributions are shown by magenta and blue lines respectively. Dashed and solid lines correspond to two different ways for modeling of complementary non-resonant contributions to $\pi\Delta$ isobar channels, described in [163]

Resonance structures are clearly seen in 2π electro-production data in entire Q^2 area

Contributing factors	Range for variation
Effective Reggeon coupling α_R [144]	15%
The magnitude for diffractive ρ-production amplitude	15%
The magnitudes of mechanisms contributed to direct 2π production [142]	10%
N^* electro-couplings	10-50%
N^* $\pi\Delta$ and ρp hadrons decay width	100-400% for the states lebeled "var" in Table 2

Table 3: Major contributors to uncertainties of N^* electro-couplings, determined from 2π exclusive channel.

covered by CLAS measurements Fig. 29. The particular feature, observed in CLAS 2π data, is growth of resonant over non-resonant mechanism ratio as photon virtuality increases.In leading order, Q^2-evolution of non-resonance mechanisms may be described by monopole fit. Such behavior reflects driving contribution from pion-in-flight Born term to non-resonant mechanisms at the intermediate Q^2<1.5 GeV^2. From CLAS data analysis we found that Q^2 evolution of $A_{1/2}$ N^* electromagnetic form factors is smoother for most excited proton states. Therefore, relative N^* signal becomes more pronounced at higher Q^2. In makes N^* studies at high photon virtualities very attractive. To compensate cross-sections fall-off with photon virtuality we need higher luminosity of CLAS12.

JM05 model was applied successfully for N^* studies from CLAS data. We determined N^* electrocouplings at photon virtualities Q^2<1.5 GeV^2 for almost all N^* of 4 and 3 star PDG status, with masses less than 2.0 GeV, from combined analysis of all available 2π unpolarized cross-sections. All these data combined were fitted within the framework of JM05. N^* electro-couplings obtained from CLAS data analysis are shown on Fig. 30. in comparison with previous world data. World data come from 1π electro-production analysis. For the states with major 1π decays, which were extensively studied previously as D13(1520), F15(1685), N^* electro-couplings, extracted in our analysis, coincide with world data. It is further evidence for capability of JM05 approach to access N^* electro-couplings. For most high lying (M>1.65 GeV) states reliable electro-couplings were obtained for the first time. Single pion exclusive channel just has not enough sensitivity to most high lying N^* with major 2π hadronic decays. This is a reason for large uncertainties in previous world data on high lying state electro-couplings. So, comprehensive studies of 2π exclusive channel are critically important to get reliable data on electro-couplings for high lying proton excitations.

The major contributors to uncertainties of N^* electro-couplings estimated within the framework of JM05 model are summarized in Table 3.

We developed special procedure to determine range of N^* electro-couplings as well as

non-resonant mechanism parameters of the Table 3 compatible to the measured observables. N^* electromagnetic form factors were fluctuated around theirs expected values, obtained in previous analysis[159]. We applied normal sampling for N^* electro-couplings with σ parameter equal to 30% from expected electro-coupling values for most electromagnetic form factors. However for well studied states as D13(1520), F15(1685) this range was reduced to 10 %, while for small and/or poorly known electromagnetic couplings fluctuation range was extended up to 50 %. Poorly known hadronic parameters for N^*, labeled in the Table 2, as "var" were also varied. Range of N^* $\pi\Delta$ and ρp hadronic coupling fluctuation was wide and causes total hadronic decay widths floating from 40 to 600 MeV. Simultaneously we fluctuated the parameters of non resonance mechanisms within the ranges listed in the Table 3. Areas adopted for fluctuation of non-resonant parameters were chosen at their upper limits compatible to measured differential cross-sections. For each trial set of JM05 parameters all single differential cross-sections were calculated. From comparison between measured and calculated single differential cross-sections χ^2/d.p. were estimated separately in each Q^2 bin and averaged over all available W-bins. We selected calculated cross-sections with χ^2/d.p. below some predetermined value, for which all calculated differential cross-sections are mostly inside the data uncertainties. N^* electro-couplings for selected in this way calculated cross-sections were averaged. Their mean value were assigned to electro-couplings extracted from the data fit, while dispersions of their distributions were treated as electro-couplings uncertainties.

We found that from available CLAS 2π data we are able to determine N^* electromagnetic form factors with accuracy 10 % or even better for largest amplitudes, while for intermediate electro-coupling values uncertainties range from 10 to 30 %.

JM05 model will be used to determine N^* electro-couplings from data on 2π electro-production at high Q^2, accessible with 11 GeV beam. It will be first step of analysis with a goal to determine ranges for N^* electro-couplings. This information will be used as input for final evaluation of N^* electromagnetic form factors and hadronic parameters within the framework of coupled channel approach, described in Sections 5.2-5.5.

Based upon capability of JM05 model to extract electro-couplings for most excited proton state from the available CLAS 2π data, we expect, that at photon virtualities covered by 11 GeV beam we will be able to determine N^* electro-couplings if:

- collected statistic will be comparable with achieved in analyzed CLAS data;
- ratio resonance over non-resonance contributions will be comparable or better than in already studied area of Q^2.

7.1.5 Feasibility for N^* studies in 2π electro-production at high still unexplored photon virtualities

To evaluate feasibility of extracting N^* electro-couplings, first we estimated ratio resonant over non-resonant contributions at photon virtualities above covered by available CLAS 2π measurements. within the framework of JM03 version [147, 148]. These calculations were

carried out within the framework of JM03 version [147, 148] for Q^2 from 1.5 to 4.0 GeV^2. At larger Q^2 we may expect significant contributions from hard processes, which involve directly quark and gluon degrees of freedom. These processes were not accessible at moderate Q^2 and were omitted in JM05. For indicative predictions we used JM03 version with 3-body phase space parametrization for remaining processes. 3-body phase space were fitted to the CLAS 2π data and extrapolated toward high Q^2, using second other polynomial for Q^2-evolution. Electro-couplings of the [70,1^-] multiplet N^* were fitted within the framework of approach [132]. A,B,C parameters of model [132] were extrapolated toward high Q^2. Using determined in this way values of A,B,C parameters, we calculated [70,1^-]-plet N^* electro-couplings at Q^2 from 1.5 to 4.0 GeV^2. Electro-couplings for the high lying states of [56,2^+]-plet as well as for $3/2^+(1720)$ candidate state were estimated based on pQCD scaling behavior.

Obtained in this way ratio resonant over non-resonant mechanisms as a function of Q^2 are shown on Fig. 32 Red lines correspond to such ratio determined from CLAS data [115]. Predictions at Q^2 from 2 to 4 GeV^2 are shown by blue lines. We are expecting steep growth of relative N^* signal from these predictions.

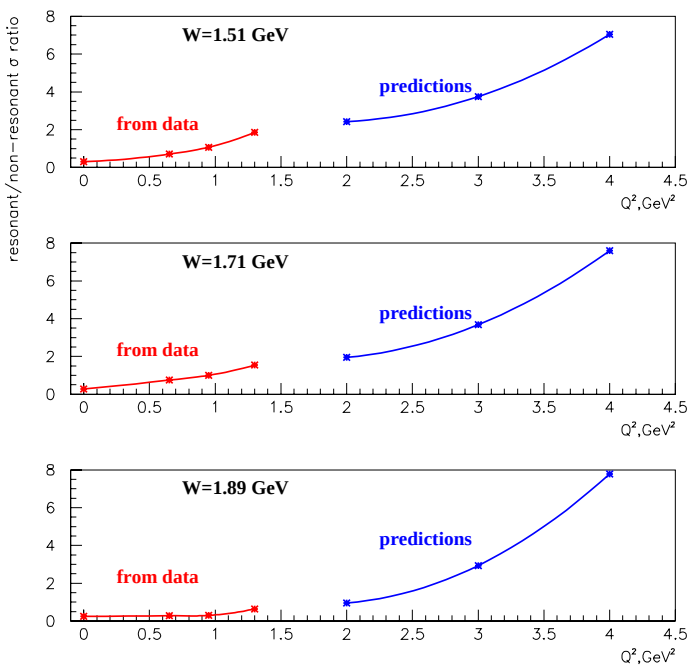

Figure 32: Ratio resonant over non-resonant mechanisms in 2π electro-production as a function of Q^2 at various W: determined from available CLAS data (red), predicted (blue).

Even if resonant over non-resonant ratio will have smoother behavior, it is difficult to expect, that this ratio at high Q^2 will be smaller, than at $Q^2 < 1.5 GeV^2$. So, conservatively, we concluded that resonant over non-resonant contribution ratio at high Q^2 will be not smaller, than extracted from CLAS data at photon virtuality 1.3 GeV^2. So N^* electro-couplings at Q^2 from 5.0 to 10.0 GeV^2 may be determined, if statistics collected in most

$W\&Q^2$ bins, covered by measurements with CLAS12 will be comparable or larger, than it was achieved in available CLAS 2π data [115],[119].

7.1.6 Simulation of 2π electro-production with CLAS12. Feasibility to study 2π exclusive channel at Q^2 from 5.0 to 10 GeV^2

We carried out the studies of resolution and acceptance of CLAS12 detector with a goal to evaluate our capabilities to obtain double charged pion electro-production cross-sections in Q^2 area from 5.0 to 10 GeV^2. In simulation we used Genova event generator [164]. For 11 GeV electron beam we simulated 2 pion and 3 pion electro-production channels. CLAS Fast MC package [165] were applied to generated events for simulation of CLAS12 response. Simulated and accepted events were studied in kinematics area over W from 1.2 to 3.5 GeV and for the photon virtualities from 5.0 to 10.0 GeV^2. For accepted 2π events we applied selection procedures and kinematics cuts similar to already used in analysis of available CLAS 2π data.

Fist, we studied capability to isolate sample with 2π events in multi pion electro-production, Distribution over $M^2_{\pi^+pX}$ missing mass squared for 2 pion and 3 pion events are shown on Fig. 33, accounting all momentum smearing expected for CLAS12.

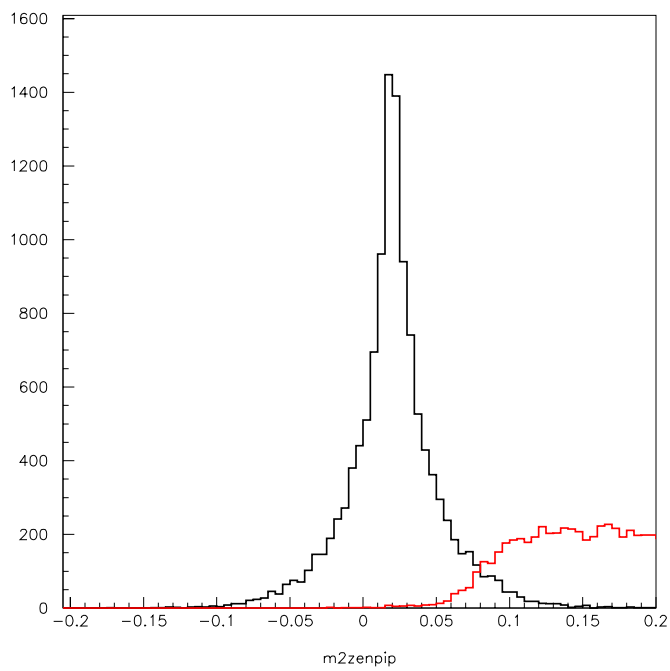

Figure 33: Distributions over $M^2_{\pi^+pX}$ for detected 2π events (black) and 3π events (red) curves.

Applying cut $M^2_{\pi^+pX} < 0.07\ GeV^2$, we will achieve reasonable isolation of 2π events with few percents multi pion contamination. Quality of multi pion background rejection may be further improved, if we restrict W range by area below 2.0 GeV, which corresponds to

major part of conventional N^*. Another way to improve multi pion rejection is to exploit correlation between missing mass squared $M^2_{\pi^+\pi^- pX}$ and missing energies for $\pi^-\pi^+p$ final hadronic system. Of course, to apply this method we need to detected all 3 final hadrons. $M^2_{\pi^+\pi^- pX}$ vs missing energy correlations are shown on Fig. 34 for 2 and 3 pion events. 2π events are situated in the spot around zero, which size is determined by mass and energy resolution. 3 pion events create strip in vertical missing energy direction. 2π event separation is pretty good, however this technique causes efficiency reduction.

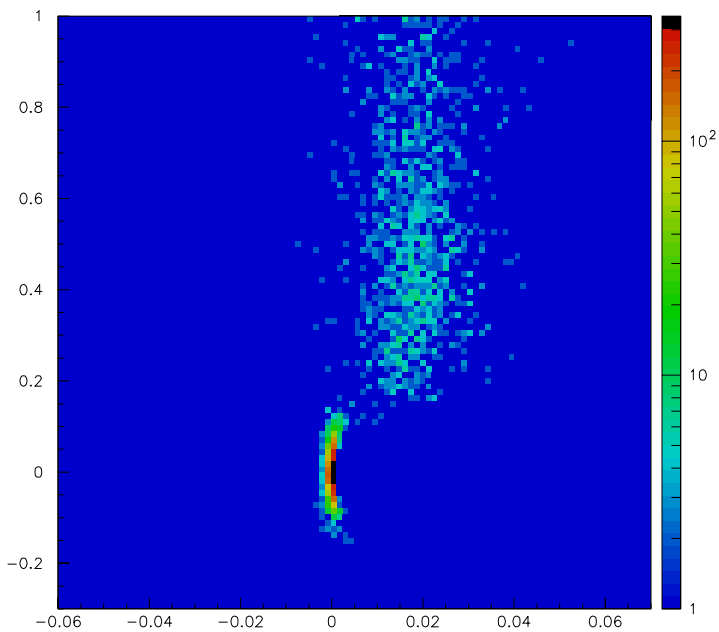

Figure 34: Separation of 2π events from multi pion background, using correlations missing energy vs $M^2_{p\pi^+\pi^- X}$. Spot around zero are 2π events. Strip in vertical dimension is created by 3 pion events.

We carried out efficiency evaluation for measurements of 2π events with CLAS12. Estimated in MC simulation efficiency for detection of 2π events, when all three final hadrons are detected is shown on Fig. 35. Efficiency is rather uniform in (Q^2& W) plane with average value 20 %. This value of efficiency was used in evaluation of counting rate.

On Fig. 36 and Fig. 37 we show efficiency for various $\pi^+\pi{-}p$ final state kinematics variables. All these efficiencies were averaged over other 4 kinematics variable for $\pi^-\pi^+p$ final state. Efficiencies were estimated in W interval from 1.5 to 1.7 GeV and averaged over photon virtualities from 5.0 to 10.0 GeV^2. Top and middle rows on Fig. 36 and Fig. 37 are generated and accepted events respectively, while efficiencies are shown at the bottom rows.

Efficiencies for various final state hadronic variables are rather flat. So, even simplest event generators may be used to estimate efficiencies in real data analysis.

Momentum resolution for final hadron are shown on Fig. 38, Fig. 39 and Fig. 40. The $(p_{rec} - p_{gen})/p_{gen}$ distributions at various particle momenta are shown. Here p_{rec} and p_{gen}

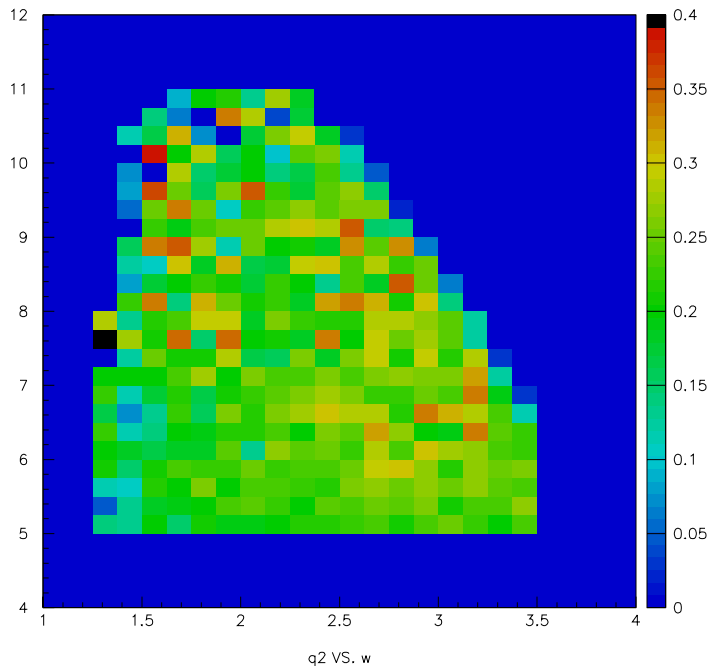

Figure 35: Efficiency for detection of 2π events with CLAS12 in (Q^2&W) plane for $\pi^+\pi^-$p detected

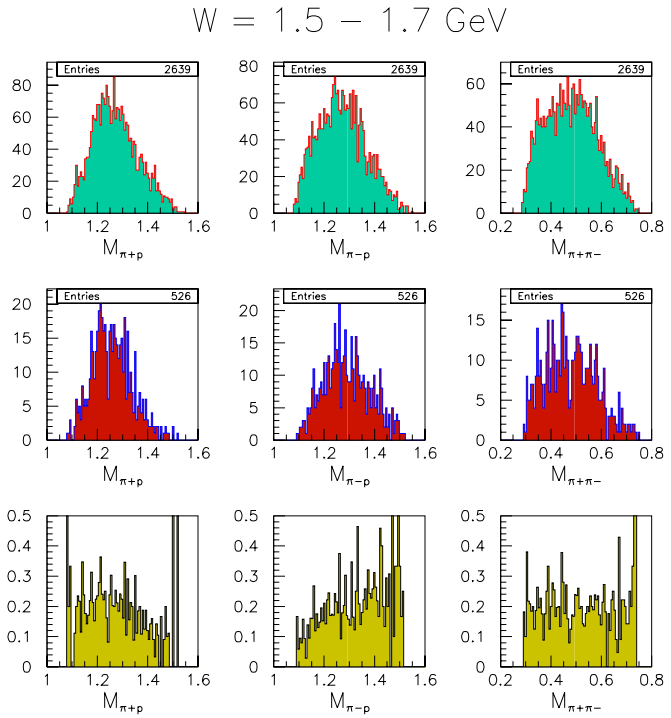

Figure 36: Efficiency for various mass distributions in 2π production at W from 1.5 to 1.7 GeV, averaged over 4 other kinematics variables and Q^2 from 5.0 to 10.0 GeV^2

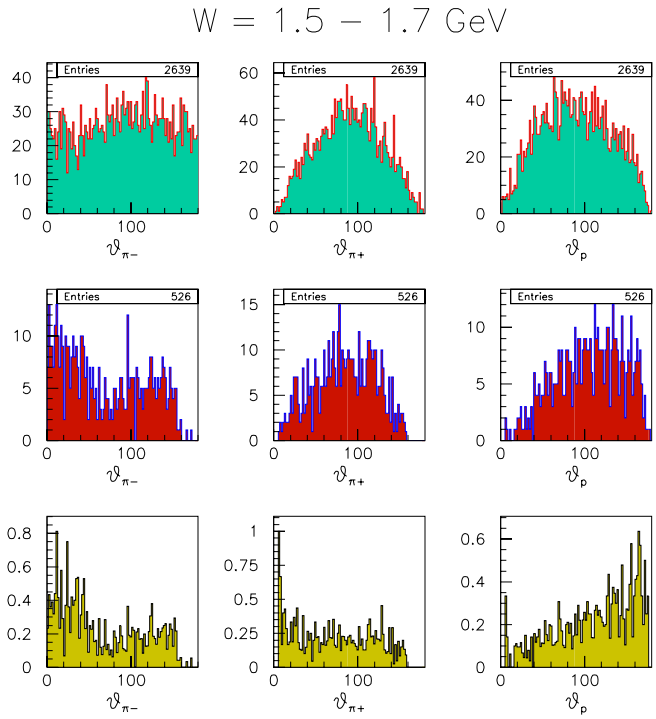

Figure 37: Efficiency for various angular distributions in 2π production at W from 1.5 to 1.7 GeV, averaged over 4 other kinematics variables and Q^2 from 5.0 to 10.0 GeV^2.

stand for momenta of reconstructed and generated hadrons respectively. Momentum resolution ranges within several percents for FWHM and rather independent from particle momenta.

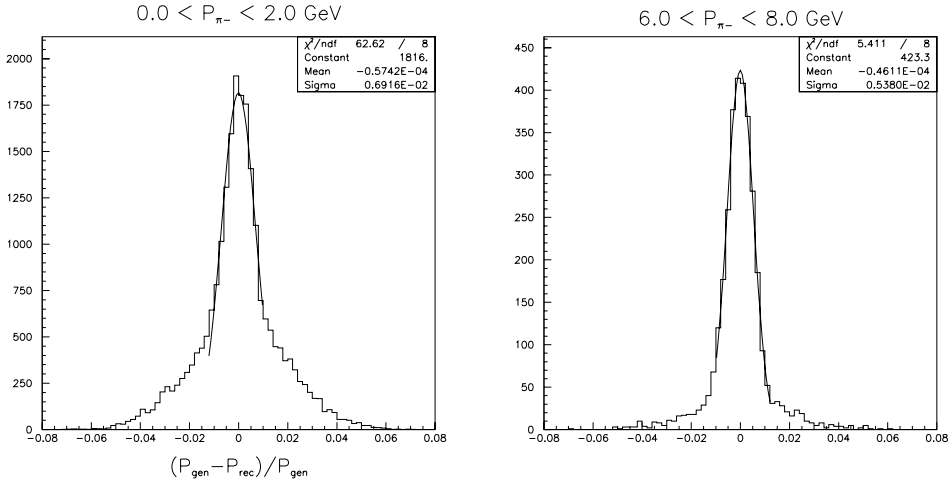

Figure 38: Momentum resolution for π^-. p_{rec}, p_{gen} are momenta for reconstructed and generated particle respectively.

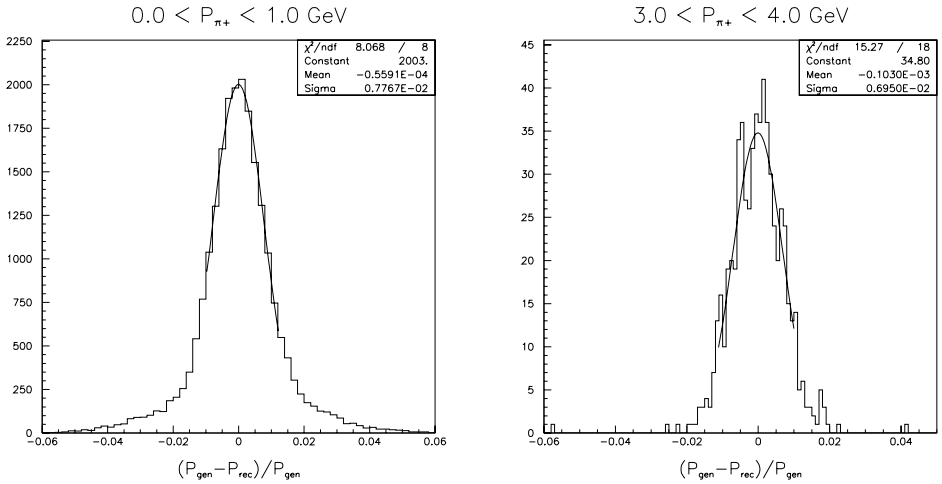

Figure 39: Momentum resolution for π^+. p_{rec}, p_{gen} are momenta for reconstructed and generated particle respectively.

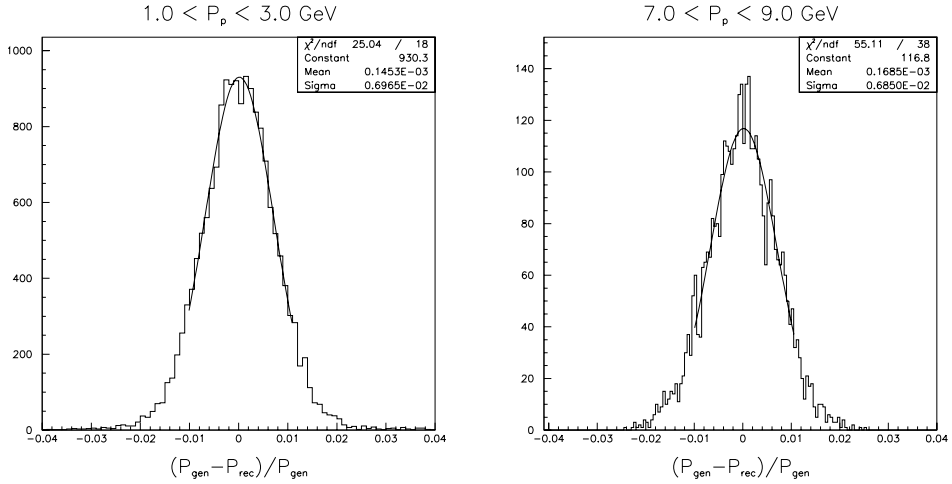

Figure 40: Momentum resolution for protons. p_{rec}, p_{gen} are momenta for reconstructed and generated particle respectively.

Using expected final particle momentum smearing for CLAS12, we estimated W-resolution, averaged over W from 1.3 to 2.0 GeV and Q^2 from 5.0 to 10 GeV^2. Calculations were carried out for two possible ways to determine W from data. First, W may be estimated from electron scattering kinematics. W resolution achieved in this way is shown on Fig. 41 as selected 2π event distribution over value $(W_{rec} - W_{gen})/W_{gen}$. Here W_{rec} and W_{gen} stand for W of reconstructed and generated events respectively.

W resolution at W range from 1.5 to 2.0 GeV is 1.5% σ value or 3.3% FWHM. This

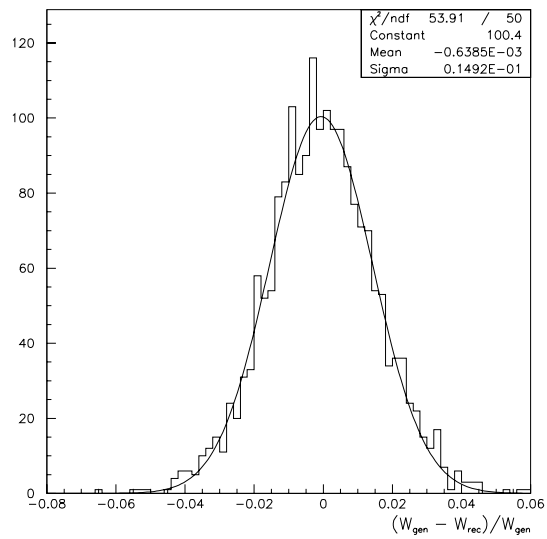

Figure 41: Resolution over W, averaged over W from 1.5 to 2.0 GeV nd over photon virtualities from 5.0 to 10 GeV^2. Invariant mass of the final hadronic system were determined from electron scattering kinematics.

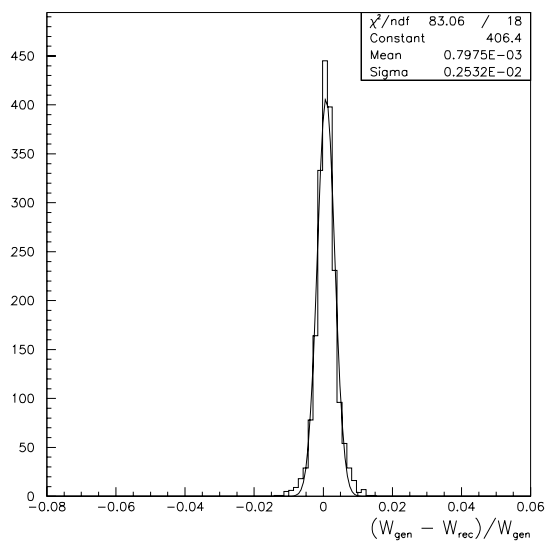

Figure 42: The same as on Fig. 41. Invariant masses of the final hadronic system were determined from the final hadron momenta.

resolution improves as W increases. However for W=1.7 GeV 3.3% FWHM corresponds to almost 60 MeV absolute value for resolution. It is comparable with total hadronic decay width of N^* in this mass range. So we tried to figure out a way to improve W resolution. We studied another possibility to determine W from four-momenta of the final hadrons. Absolute value of the final hadron momenta are defined by W. So, at $W < 2.0$ GeV absolute

value for hadron momenta smearing should me much less, then for scattered electron of 7-10 GeV momenta, corresponded to N^* excitation. Therefore, we may expect improvement in W-resolution, if W value would be calculated from the final hadron momenta. W resolution achieved in this way is shown on Fig. 42 For W from 1,3 to 2.0 GeV we have considerable improvement. FWHM fall down from 3.3% to 0.6%.

So, we are going to determine W value from three momenta of the final hadrons. In this case we may adopt size of W-cell 25 MeV. This size of W-cell was used for evaluation of counting rate, while size over Q^2 was determined by requirement to collect proper statistic during experimental run and chosen equal to 0.5 GeV^2.

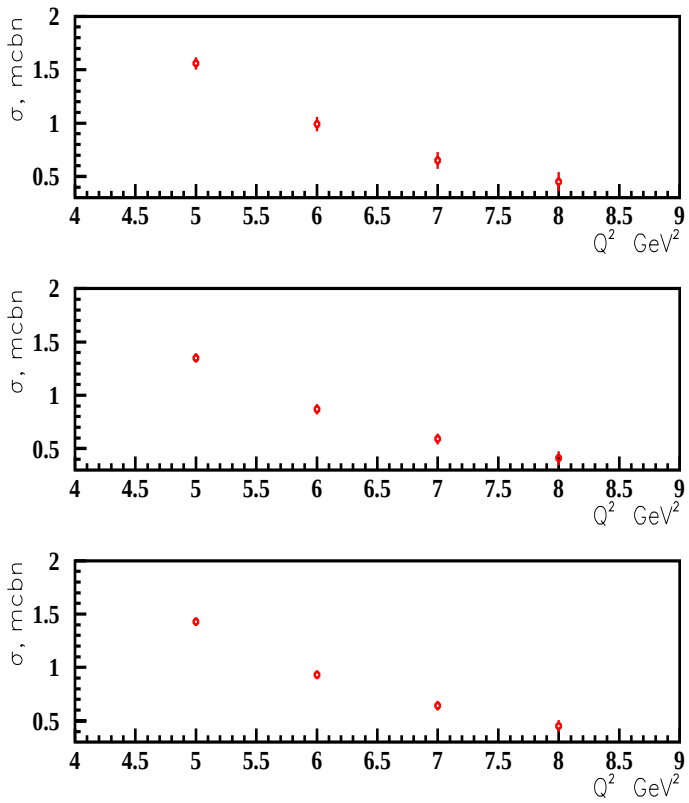

Figure 43: Total 2π cross-sections at photon virtualities from 5.0 to 10.0 GeV^2, estimated from the data on inclusive structure function F_2 [166]. W=1.71 GeV (top), W=1.84 GeV (middle), W=1.89 GeV (bottom)

To estimate counting rate, we need some evaluation for double charged pion cross-sections at Q^2 from 5.0 to 10.0 GeV^2. In this kinematics area we unable to use JM05 even as a guide, since at this high photon virtualities hard mechanisms may modify considerably non-resonant processes in JM05, established from the CLAS data fit at $Q^2 < 1.5 GeV^2$. So, we

accepted another approach for indicative estimates of total 2π cross-sections. As a starting point we used fit of inclusive structure function proposed in [166]. This fit works pretty good at Q^2<10.0 GeV^2 in N^* excitation region. From this fit we estimated total inclusive cross-section under virtual photons. To obtain 2π total cross-sections, we used ratio 2π cross-section over inclusive virtual photon cross-section. This ratio was taken from CLAS data at $Q^2 < 1.5 GeV^2$ and extrapolated to the Q^2 area from 5.0 to 10.0 GeV^2. Estimated in this way total 2π cross-sections at several W values are shown on Fig. 43.

We used average efficiency value for detection of 2π events 20%, estimated with CLAS12 Fast MC.

The number of collected events as described above (Q^2&W) cells is shown on Fig. 44 for 60 days run time.

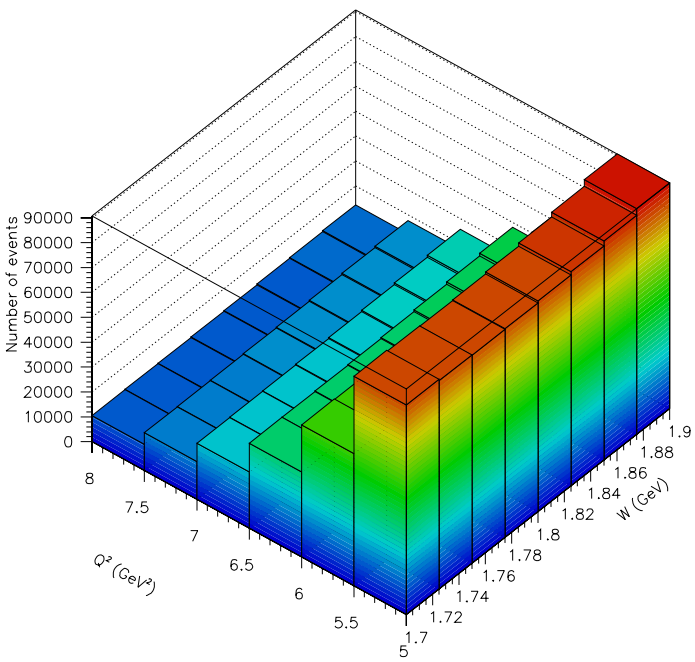

Figure 44: Number of collected 2π events in N^* excitation region with CLAS12. 60 days run time. 10^{35} $cm^{-2}s^{-1}$ luminosity.

In analysis of available CLAS 2π data [115, 119] we needed statistic above 10000 events for most (Q^2&W) cells, to obtain entire set of 2π single differential cross-sections, described in Section 7.1.1. As it follow from Fig. 44, counting rate for 2π events with CLAS12 will be sufficient to produce cell population >10000 2π events in W area from 1.7 to 1.9 GeV and likely in overall N^* excitation region, based on available data both on W-dependence of 2π integrated cross-sections and inclusive structure functions.

8 Projected N^* Electro-Coupling, Expected from Proposed Experiments

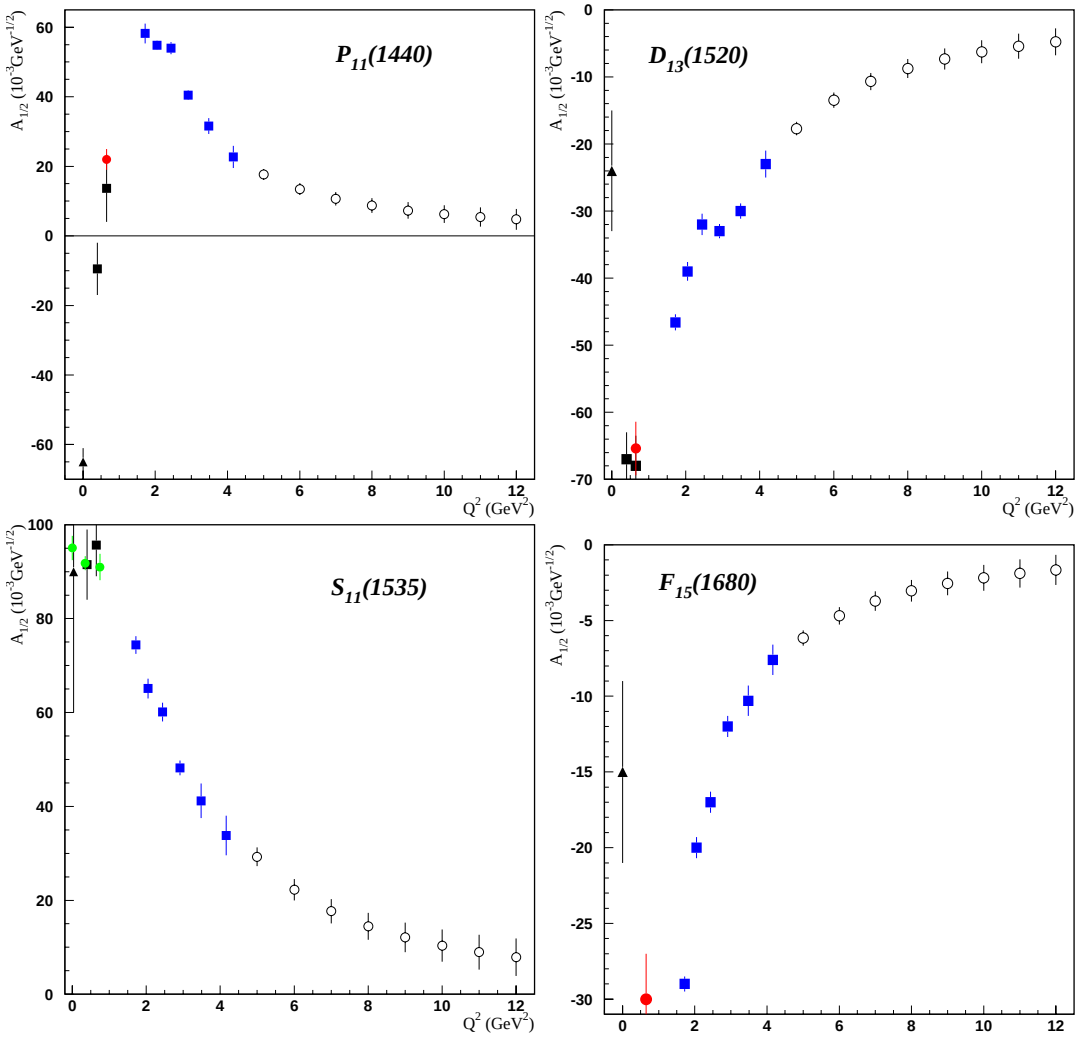

Figure 45: Projected N^* electro-coupling, expected in proposed experiments (open circles with error bars) . We also present electro-couplings extracted from available CLAS data on 1π electro-production [36] (black filled squares), preliminary data from analysis of e1-6 run (blue filled squares) as well as the results from combined analysis of 1π and 2π electro-production [52].

In this section we demonstrate expected capability of proposed experiment to measure N^* electro-couplings for various states, which were already studied with CLAS at photon virtualities up to 4.5 GeV^2. In Fig. 45 we have presented the projected values of $A_{1/2}$ helicity amplitudes for the electro-excitation of the resonances $P_{11}(1440)$, $D_{13}(1520)$, $S_{11}(1535)$, and $F_{15}(1680)$ at $5 < Q^2 < 12$ GeV^2. These values are shown along with the existing results

at smaller Q^2. The projected values of helicity amplitudes are obtained via continuation of the results at $Q^2 = 2.91 - 4.16\ GeV^2$ according to pQCD behavior $A_{1/2} \sim Q^3$. As it was demonstrated in Fig. 5 such assumption can be applied to the helicity amplitudes of the $P_{11}(1440)$, $D_{13}(1520)$, $S_{11}(1535)$, and $F_{15}(1680)$. The presented errors of projected amplitudes are obtained supposing that the relative errors and amount of data will be close to those obtained in the CLAS experiments for π^+ electro-production at Q^2 from 1.72 to 4.16 GeV^2.

9 Summary and Beam Time Request

In recent years the CLAS Collaboration has succeeded to determine the Q^2 evolution of baryon resonance electro-coupling amplitudes from unpolarized single- and double-pion electroproduction data. Consistent results for both channels have been extracted by three different models, the Unitary Isobar Model (UIM) [51, 53], a dispersion theoretical approach [51, 53], and the JLab-MSU isobar model (JM05) [142]. Most of these results are still preliminary, but in the final stage of analysis, which undoubtedly shows that we are able to extract resonance parameters with unprecedented accuracy for many excited states in the mass and four momentum transfer region below $W < 1.7\,GeV$ and $Q^2 < 4.5\,GeV^2$ for single-pion (e1-6 run period) and below $W < 2.0\,GeV$ and $Q^2 < 1.5\,GeV^2$ for double-pion final states (e1 run period).

Within the total requested beam time of $60\,days$ at $11\,GeV$ electron beam energy with the highest possible electron beam polarization, the estimated collected statistics in most of the Q^2 and W bins will be higher and for the highest Q^2 bins comparable to the statistics accumulated in the previous e1 and e1-6 run periods. Furthermore the new results show that the overall resonance to background ratio increases with increasing Q^2. Therefore we are confident that we will be able to extract the resonance electro-coupling amplitudes up to typically $12\,GeV^2$ by using the established model approaches applied to the same number of measured observables, which has been shown to be sufficient for this analysis.

Beam Time Request	Beam	Beam Energy	Luminosity	Target	Detector
$60\,days$	*polarized* e^-	$11\,GeV$	$10^{35}\,cm^{-2}s^{-1}$	LH_2	*base equipment*

Bibliography

[1] M. Gell-Mann, Phys. Lett. 8, 214 (1964)

[2] G. Zweig, CERN Report 8182/TH-412 (1964) (unpublished).

[3] H.L. Anderson, E. Fermi, E. A. Long, D.E. Nagle, Phys. Rev. 85, 936 (1952).

[4] O. W. Greenberg, Phys. Rev. Lett. 13, 598 (1964).

[5] S. Eidelmann et al. [Review of Particle Properties], Phys. Lett. B592 (2004).

[6] H. Ichie, V. Bornyakov, T. Steuer, G. Schierholz, hep-lat/0212024 (2002).

[7] T. T. Takahashi, H.Suganuma, Phys.Rev.,D70:074506 (2004).

[8] G. S. Bali, et. al., Phys.Rev.,D71:114513 (2005).

[9] A. D. Martin, et. al., Eur.Phys.J.C35, 325 (2004).

[10] E. Leader, et. al., Eur.Phys.J.C23, 479 (2002).

[11] W. Melnitchouk, R. Ent and C. Keppel, Phys. Rept. 406, 127 (2005).

[12] H. Iida, et. al., Nucl.Phys.Proc.Suppl. 141,191 (2005).

[13] G. Laveissiere et al., Phys. Rev. C **69** 045203 (2004).

[14] R.A. Arndt et al., nucl-th/9708006 (1997) and Phys. Rev. C **66**, 055213 (2002).

[15] Q.B. Li, D.O. Riska, nucl-th/0605076

[16] R. Petronzio, et. al., Phys.Rev.,D67:094004 (2003).

[17] A.V. Sidorov, C. Weiss, Phys.Rev.,D73:074016 (2006).

[18] D. Diakonov, V. Petrov, Phys. Lett. B147, 351 (1984).

[19] V. D. Burkert and T.S. Lee, Int. J. Mod. Phys. E13, 1035 (2004), nucl-ex/0407020.

[20] C. Alexandrou et al., Phys.Rev.D69:114506 (2004).

[21] C. Alexandrou et al., hep-lat/0409122.

[22] K. Goeke, M. V. Polyakov and M. Vanderhaeghen, Prog. Part. Nucl. Phys. **47**, 401 (2001) [arXiv:hep-ph/0106012].

[23] L. L. Frankfurt, M. V. Polyakov, M. Strikman and M. Vanderghehgan. Phys. Rev. Lett. **84**, 2589 (2000)

[24] S. S. Kamalov and S.N. Yang, Workshop N*2000, World Scientific (2001).

[25] C. Mertz et al., Phys. Rev. Lett. 86, 2963 (2001).

[26] E. Pace, G. Salme, and S. Simula, Few Body Syst. Suppl. 10:407 (1999).

[27] M. Aiello, M.M. Giannini, and E. Santopinto, J. Phys. G24, 753 (1998).

[28] F. Cano and P. Gonzales, Phys. Lett. B431:270 (1998).

[29] T. Sato and T.S. Lee, Phys. Rev. C63:055201, 2001.

[30] D. O. Riska, Talk at MENU2004, Beijing (2004).

[31] A. Matsuyama, T. Sato, and T.-S. H Lee, to be submitted to Phys. Report (2006)

[32] A. Matsuyama, Phys. Lett. **B152**, 42 (1985)

[33] T. Sato and T.-S. H. Lee, Phys. Rev. **C54**, 2660 (1996); **C63**, 055201 (2001)

[34] M. Paris, Phys. Rev. Lett. **95**, 202002 (2005)

[35] B. Julia-Diaz, B. Saghai, T.-S. H. Lee, and F. Tabakin, Phys. Rev. **C73**, 055204 (2006)

[36] I.G.Aznauryan et al., Phys.Rev. **C71**, 015201 (2005)

[37] B. Julia-Diaz, T.-S. H. Lee, A. Matsuyama, M. Paris, and T. Sato, in progress

[38] K. Nakayama et al., in progress

[39] V.V. Frolov *et al.*, Phys. Rev. Lett. **82** (1999) 45.

[40] J. Volmer *et al.*, Phys. Rev. Lett. **86** (2001) 1713.

[41] M.K. Jones *et al.*, Phys. Rev. Lett. **84** (2000) 1398.

[42] O. Gayou *et al.*, Phys. Rev. Lett. **88** 092301 (2002).

[43] D.J. Hamilton *et al.*, Phys. Rev. Lett. **94** 242001 (2005).

[44] N. Isgur, S. Jeschonnek, W. Melnitchouk and J. W. Van Orden, Phys. Rev. D 64, 054005 (2001).

[45] F. E. Close and W. Melnitchouk, Phys. Rev. C 68, 035210 (2003).

[46] M. Aiello *et al.*, J. Phys. G **24** (1998) 753.

[47] L. Andivahis *et al.*, Phys. Rev. D **50** (1994) 5491.

[48] R.G. Arnold *et al.*, Phys. Rev. Lett **57** (1986) 174.

[49] I.G. Aznauryan and K. Oganessyan, Phys. Lett. B **249** (1990) 309.

[50] I.G. Aznauryan, Phys. Rev. C **68** 065204 (2003).

[51] I.G. Aznauryan, Phys. Rev. C **67** 015209 (2003).

[52] I.G. Aznauryan *et al.*, Phys. Rev. C **72** 045201 (2005).

[53] I.G. Aznauryan, in preparation (2006).

[54] W. Bartel *et al.*, Nucl. Phys. B **58** (1973) 429.

[55] Ch. Berger *et al.*, Phys. Lett. B **35** (1971) 87.

[56] C. J. Bebek *et al.*, Phys. Rev. D **13** (1976) 25.

[57] C. J. Bebek *et al.*, Phys. Rev. D **17** (1978) 1693.

[58] R. Beck *et al.*, Phys. Lett. C **61** 035204 (2000).

[59] E.D. Bloom *et al.*, Phys. Rev. Lett **23** (1969) 930.

[60] A. Bodek *et al.*, Phys. Rev. D **20** (1979) 1471.

[61] P. Bosted *et al.*, Phys. Rev. C **51** (1995) 718.

[62] P.O. Bowman *et al.*, Phys. Lett. D **66** 014505 (2002) and arXiv:hep-lat/0209129 (2002).

[63] M. Breidenbach *et al.*, Phys. Rev. Lett **23** (1969) 935.

[64] F. W. Brasse *et al.*, DESY 76/11 (1976).

[65] F. W. Brasse *et al.*, Nucl. Phys. B **110** (1976) 410.

[66] F. W. Brasse *et al.*, Z. Phys. C **22** (1984) 33.

[67] S.J. Brodsky and G.P. Lepage, Phys. Lett. B **87** (1979) 359.

[68] S.J. Brodsky and G.P. Lepage, Phys. Rev. D **22** (1980) 2157.

[69] V.M. Braun *et al.*, Phys. Lett. D **73** 034020 (2006).

[70] V. D. Burkert, T.-S.H. Lee, Int. J. Mod. Phys. E **13** (2004) 1035.

[71] S. Capstick and B.D. Keister, Phys. Rev. D **51** (1995) 3598.

[72] F. Cano and P. Gonzalez, Phys. Lett. B **431** (1998) 270.

[73] V.L. Chernyak and A.R. Zhitnitsky, JETP Lett. **25** (1977) 510; V.L. Chernyak, A.R. Zhitnitsky and V.G. Serbo, JETP Lett. **26** (1977) 594.

[74] J.C. Collins *et al.*, Phys. Rev. D. **56** (1997) 2982.

[75] D. Day, arXiv:nucl-ex/0502003.

[76] D. Drechsel *et al.*, Nucl. Phys. A **645** (1999) 145.

[77] H. K. Egiyan *et al.*, Phys. Rev. C **73** 025204 (2006).

[78] V. Eletski and Ya. Kogan, Yad. Fiz. **39** (1984) 138.

[79] O. Gayou *et al.*, Phys. Rev. C **64** 038202 (2001).

[80] R.W. Gothe *et al.*, Proc. NSTAR 2002, Pittsburgh, PA, World Scientific (2003) 220.

[81] R. Hofstadter and R.W. McAllister, Phys. Rev. **98** (1955) 183 and Phys. Rev. **102** (1956) 851.

[82] X. Ji, Phys. Rev. Lett. **78** (1997) 610 and Phys. Rev. D. **55** (1997) 7114.

[83] X. Ji *et al.*, Phys. Rev. Lett. **90** 241601 (2003).

[84] K. Joo *et al.*, Phys. Rev. Lett. **88** 122001 (2002).

[85] K. Joo *et al.*, Phys. Rev. C **68** 032201 (2003).

[86] K. Joo *et al.*, Phys. Rev. C **70** 042201 (2004).

[87] S.S. Kamalov *et al.*, Phys. Lett. C **64** 032201 (2003).

[88] C. Keppel, Ph. D thesis, American University, Washington, DC (1994).

[89] J.J. Kelly *et al.*, Phys. Rev. Lett. **95** 102001 (2005).

[90] I.S. Barker, A. Donnachie and J.K. Storrow, Nucl. Phys. B **95** (1975) 347.

[91] J. Litt *et al.*, Phys. Lett. B **31** (1970) 40.

[92] Z. Li and V. Burkert, Phys. Rev. D **46** (1992) 70.

[93] A. Lung *et al.*, Phys. Rev. Lett. **70** (1993) 718.

[94] C. Mertz *et al.*, Phys. Rev. Lett. **86** (2001) 2963.

[95] D. Mueller *et al.*, Fortschritte der Physik **42** (1994) 101.

[96] E. Pace *et al.*, Few Body Syst. Suppl. **10** (1999) 407.

[97] K. Park *et al.*, to be submitted to Phys. Rev. C (2006).

[98] C.E.Carlson and J. Poor, Phys. Rev. D **38**, (1988) 2758.

[99] S. Eidelman *et al.*, Phys. Lett. B **592**, (2004) 1.

[100] S. Poucher *et al.*, Phys. Rev. Lett. **32**, (1974) 118.

[101] L. E. Price *et al.*, Phys. Rev. D **4** (1971) 45.

[102] A.V. Radyushkin, Phys. Rev. B **380** (1997) 417.

[103] S. Rock *et al.*, Phys. Rev. Lett. **49** (1982) 1139.

[104] S. Rock *et al.*, Phys. Rev. D **46** (1992) 24.

[105] T. Sato and T.S.H. Lee, Phys. Lett. C **54** (1996) 2660.

[106] M.A. Shifman, A.I. Vainshtein, V.I. Zakharov, Nucl. Phys. **B147** (1979) 385.

[107] A. F. Still *et al.*, Phys. Rev. D **48** (1993) 29.

[108] P. Stoler, Phys. Rep. **226** (1993) 103.

[109] P. Stoler, Phys. Rev. Lett. **91** 172303 (2003).

[110] M. Ungaro *et al.*, CLAS, to be submitted to Phys. Rev. Lett. (2006).

[111] R. L. Walker, Phys. Rev. **182** (1969) 1729.

[112] M. Warns *et al.*, Z. Phys. C **45** (1990) 627.

[113] R. C. Walker *et al.*, Phys. Rev. D **49** (1994) 5671.

[114] M.K. Jones *et al. Phys. Rev. Lett.* **84**,1398 (2000); O. Gayou *et al. Phys. Rev.* **C64**,038202 (2001).

[115] M. Ripani, et. al., Phys. Rev. Lett. **91**, 022002 (2003).

[116] M.Bellis, et.al. (CLAS Collaboration), Proceedings of NSTAR2004 workshop , March 24-27, 2004, Grenoble, France, World Scientific, ed. by J.-P. Bocquet, V. Kuznetsov, D. Rebreyend, 139.

[117] M. Battaglieri, et. al. Phys. Rev. Lett. **87**, 172002 (2001).

[118] S. Strauch, et. al.,Phys. Rev. Lett., accepted, hep-ex/0508002.

[119] G. Fedotov, et. al., CLAS Analysis Note, June2006

[120] U. Thoma, Int. J. Mod. Phys. **A20**, 280 (2005).

[121] C. Wu, et. al. Eur. Phys. J **A23**, 317 (2005).

[122] Y. Assafiri, et. al., Phys. Rev. Lett. **90**, 222001 (2003).

[123] J. Ahrens, et. al., Phys. Lett. **B624**, 173 (2005).

[124] J. Ahrens, et. al., Phys. Lett. **B551**, 49 (2003).

[125] M. Kotulla, et. al., Phys. Lett. **B578**, 63 (2004).

[126] W. Langgartner, et. al., Phys. Rev. Lett. **87**, 052001-1 (2001).

[127] F. Harter, et. al., Phys. Lett. **B401**, 229 (1997).

[128] A. Braghieri, et. al., Phys. Lett. **B363**, 46 (1995).

[129] Review of Particle Physics, S. Eidelman et al., Phys. Lett. **B592**, 1 (2004).

[130] L. Tiator, et. al., Eur. Phys. J **A19**, 55 (2004).

[131] D. Merten, et. al., Eur. Phys. J **A14**, 477 (2002).

[132] V. D. Burkert, et. al., Phys. Rev. **C67**, 035204 (2003).

[133] I. G. Aznauryan, et. al., Yad. Fiz. **41**, 249 (1985).

[134] R. Jaffe, F. Wilczek., Phys. Rev. Lett. **91**, 232003 (2003).

[135] F. Wilczek, arXiv:hep-ph/0406168.

[136] Q. Zhao, F.E.Close, arXiv:hep-ph/0605336.

[137] M. M. Giannini, et. al., Phys. Rev. **C72**, 0220201(R) (2005).

[138] J. Chizma, G. Karl, Phys. Rev.**D68**, 054007 (2003).

[139] L. Glozman, Nucl. Phys, **A755**, 17 (2005).

[140] S. Capstick, W. Roberts., Prog. Part. Nucl. Phys. **45**, S241 (2000).

[141] L. Glozman, Int. J. Mod. Phys. **A21**, 475 (2006).

[142] V. Mokeev, et. al., arXiv:hep-ph/0512164.

[143] Cambridge Bubble Chamber Group, Phys. Rev. 155, 1477(1967); ABBHHM Collaboration, Phys. Rev. 175, 1669 (1968).

[144] M. Ripani et. al., Nucl. Phys, **A672**, 220 (2000).

[145] M. Ripani et. al., Phys, of Atom. Nucl. **63**, 1943 (2000).

[146] V. Mokeev et. al., Phys, of Atom. Nucl. **64**, 1292 (2001).

[147] V. Mokeev et. al., Phys, of Atom. Nucl. **66**, 1322 (2003).

[148] V. Burkert et. al., Phys, of Atom. Nucl. **66**, 2149 (2003).

[149] A. Anisovich, et. al., Eur. Phys. J **A24**, 111 (2005).

[150] D. Luke and P. Soding, Springer Tracts in Mod. Phys. **59** (1971).

[151] A. Bartl, W. Majerotto, D. Schildknecht, Nuovo Cimento 12A, 703(1972).

[152] L.Y. Murphy, J.M. Laget, DAPNIA-SPHN-96-10, Mar. 1996.

[153] W. Roberts, JLAB-THY-97-01, (1997).

[154] W. Roberts, T. Oed, Phys. Rev., C **71**, 055201 (2005).

[155] J.A. Gomez-Tejedor and E. Oset, Nucl.Phys. A571, 667(1994); J.A. Gomez-Tejedor and E. Oset, Nucl.Phys. A600(1996).

[156] J.C Nacher et. al., Nucl. Phys, **A695**, 295 (2001).

[157] J.C Nacher et. al., Nucl. Phys, **A697**, 372 (2002).

[158] K. Ochi, M. Hirata, T. Takahi, Phys. Rev., C56, 1472(1997).

[159] V.D. Burkert, et. al., Proc. of the 17 International UPAP Conference on Few-Body Problems in Physics, Durham. NC, USA, 5-10 June 2003, Elsevier, 2004, ed.by W. G. Glöckle, W. Tornow, S231.

[160] D.G. Cassel, et. al., Phys. Rev. **D24** 2787 (1981).

[161] N.V. Shvedunov, et. al., accepted by Physics of Atomic Nuclei

[162] H.Avakyan, et. al, CLAS12 Proposal

[163] V.I. Mokeev, presentation at CLAS Collaboration Meeting, http://www.jlab.org/ mokeev/CLAS030206.ppt

[164] M. Ripani and E.N. Golovach based on P. Corvisiero et al., NIM A **346**, (1994) 433.

[165] CLAS12 Fast MC

[166] L. W. Witlow, et. al., Phys. Lett. **B282** 475 (1992).